Security Classification of This Report Has Been Cancelled

[redacted]

[redacted]

Copy
RM L52D30

TECH LIBRARY KAFB, NM
0144459

NACA RM L52D30

7331

[redacted]

NACA

RESEARCH MEMORANDUM

PRESSURE DISTRIBUTIONS ON BODIES OF REVOLUTION AT SUBSONIC AND TRANSONIC SPEEDS

By Richard I. Cole

Langley Aeronautical Laboratory
Langley Field, Va.

Classification cancelled (or changed to Unclassified)
By authority of NASA Tech Pub Announcement 74 30 Nov 54
(OFFICER AUTHORIZED TO CHANGE)
By ..... NAME OF
GRADE OF OFFICER MAKING CHANGE)
10 Apr 61
DATE

CLASSIFIED DOCUMENT
This material contains information affecting the National Defense of the United States within the meaning

[redacted]

NATIONAL ADVISORY COMMITTEE
FOR AERONAUTICS
WASHINGTON
July 21, 1952

"Receipt signature required"

319.98/13

[redacted]

[redacted]

Security Classification of This Report Has Been Cancelled

TECH LIBRARY KAFB, NM
0144459

NATIONAL ADVISORY COMMITTEE FOR AERONAUTICS

RESEARCH MEMORANDUM

PRESSURE DISTRIBUTIONS ON BODIES OF REVOLUTION AT SUBSONIC AND TRANSONIC SPEEDS

By Richard I. Cole

SUMMARY

Pressure distributions measured along prolate spheroids of fineness ratios 3 to 20 and along a slender body of fineness ratio 12 are compared at subsonic and transonic speeds with estimated distributions for several angles of attack. The comparisons showed that the pressure distributions along the bodies can be predicted with fair accuracy.

INTRODUCTION

In response to recent demands for pressure-distribution data on bodies of revolution at high subsonic Mach numbers through a large angle-of-attack range, an investigation has been conducted in the Langley 24-inch high-speed tunnel at high-subsonic Mach numbers on a series of prolate spheroids of fineness ratios 3 to 20, at angles of attack up to 20°. Other bodies of revolution tested in this investigation were the hemispherical-nose body, the ogive-cylinder body, and the parabolic body.

The purpose of this paper is to present experimental pressure-distribution data from the 24-inch-tunnel investigation and from references 1 to 3 and to examine the adequacy of various existing methods for estimating these data. A comparison of 24-inch-tunnel data and data from references 4 and 5 is also presented for Reynolds number evaluation.

SYMBOLS

f	fineness ratio, $l/2r_{max}$ (see fig. 1)
l	total length of basic body (see fig. 1)
M	free-stream Mach number

HAFB 1289

Security Classification of This Report Has Been Cancelled

p	static pressure
P	pressure coefficient, $\frac{p_l - p_s}{q_s}$
ΔP	incremental pressure coefficients at a given station due to angle of attack, $P - P_{\alpha=0^\circ}$
$P_{\alpha=0^\circ}$	pressure coefficient at zero angle of attack
q	dynamic pressure
r	local radius of body (see fig. 1)
R	Reynolds number based on body length
x	coordinate along major axis of body (see fig. 1)
α	angle of attack
θ	polar angle about axis of revolution measured from velocity-approach direction

Subscripts:

c	compressible value
cr	critical value
i	incompressible value
l	local conditions, as on model surface
max	maximum value
s	free-stream condition

MODELS

The profiles, location of pressure orifices, and other pertinent data for the bodies tested are presented in figure 1. The ordinates of the hemispherical-nose body, the ogive-cylinder body, the parabolic body, and the modified-parobolic body are presented in table I.

Security Classification of This Report Has Been Cancelled

The models were supported by a hollow sting which enclosed the leads from the surface-pressure orifices. The 1-inch-diameter prolate spheroid, the hemispherical-nose body, and the parabolic body had 14 to 17 pressure orifices installed along one meridian in the model surface (see fig. 1). The ogive-cylinder body had 15 surface-pressure orifices. The small diameter of the sting on the 0.5-inch-diameter prolate spheroids permitted only 8 orifice leads to be passed through the sting. In order to obtain the complete pressure distribution for these models, it was necessary first to measure the pressures at 8 orifices located along the rear portion of the body, and then to repeat the tests, measuring the pressures at 8 orifices located along the forward portion of the body in the same meridian. The prolate spheroids of fineness ratios 3, 5, 6, and 10 (1-inch-diameter body) had orifices located at meridians 90° apart around the 25-percent-body-length station in order to check symmetry.

APPARATUS AND TESTS

The test section of the Langley 24-inch high-speed tunnel (ref. 6), which was originally circular (24-inch diameter), was modified by the installation of flats on the tunnel walls. These flats reduced the width of the tunnel at the test section from 24 inches to 18 inches and changed the shape of the test section from circular to one more nearly approaching a rectangle. An enclosure was installed around the tunnel so that the dry air from the induction jet would mix with the air contained within the enclosure and thereby lower the humidity for more favorable testing conditions.

The test section and model support apparatus are shown in figure 2. The model sting was attached to a 3-inch-chord, 10-percent-thick support strut. This strut extended through the tunnel wall at a point 15 inches downstream of the test section and was attached to a mechanism for changing the angle of attack.

Pressure distributions were obtained along the 0° and 180° meridians of all the bodies for angles of attack from 0° to 20° at Mach numbers from 0.30 to 0.90. Pressure distributions were also obtained along the 45°, 90°, and 135° meridians of the prolate spheroids of fineness ratio 5 and 10 at an angle of attack of 6°. The Reynolds number for these tests varied from 170,000 per inch at a Mach number of 0.30 to 384,000 at a Mach number of 0.9.

Security Classification of This Report Has Been Cancelled

PRECISION

In the operation of the 24-inch high-speed tunnel it is difficult to obtain data at predetermined values of Mach number. It was therefore necessary to cross-plot the data from the various tests in order to obtain data at comparable Mach numbers. The estimated inaccuracy of the resulting data was ±0.010 in pressure coefficient and ±0.005 in Mach number.

The inaccuracy in setting the zero angle of attack is small, since the pressures at the 0°, 90°, 180°, and 270° meridians were almost the same. Changes in angle of attack could be set within 0.01°. The model deflection was calculated to be of the order of 1 percent of the angle of attack.

Wall-interference corrections for these bodies were determined by the methods presented in reference 7. At a Mach number of 0.90 the order of magnitude of these corrections was 1.007M and 1.007q for the fineness-ratio-10 prolate spheroid. Since these corrections were very small, they were not applied to the data reported herein.

Pressures measured along the tunnel walls during these tests showed that the tunnel choked on the support strut about 15 inches downstream of the model. These measurements showed that the choking phenomenon did not affect the conditions at the test section.

RESULTS AND DISCUSSION

Experimental Results

Effect of Reynolds number.- Data have been obtained for the prolate spheroids of fineness ratio 6 and 10 in the Langley 8-foot high-speed tunnel (refs. 4 and 5) at Reynolds numbers from 6.4×10^6 to 13.1×10^6, and in the Langley 24-inch high-speed tunnel at Reynolds numbers from 1.7×10^6 to 3.8×10^6. A comparison of these data at Mach numbers of 0.7 and 0.9 for an angle of attack of 0° is shown in figure 3(a). These data are in good agreement and indicate that within the range of the tests the effect of Reynolds number on the measured pressures is small.

The 24-inch-tunnel data on two bodies of fineness ratio 10 at an angle of attack of 10° are compared in figure 3(b) at Mach numbers of 0.7 and 0.9. These data are in very good agreement except possibly near the nose on the 180° meridian and near the rear of the body along both

Security Classification of This Report Has Been Cancelled

meridians. At the rear of the body the disagreement is attributed primarily to the varying influence of the sting on the pressures of the two models and possibly to some Reynolds number effects. The results indicate that the effects of Reynolds number on the measured pressure distributions are small.

Effect of Mach number, angle of attack, and body shape.- The general effects of Mach number, body shape, and angle of attack for all the bodies tested are presented in figures 4, 5, 6, and 7. For the fineness-ratio-3 prolate spheroid (fig. 4(a)), the pressure distributions at Mach numbers of 0.30 and 0.60 are almost the same at angles of attack of 0°, 10°, and 20°. At a Mach number of 0.90, the local velocities along the central portion of the body are above sonic for all angles of attack presented herein. At an angle of attack of 0°, the peak pressures are occurring near the 0.5 station. Increasing the angle of attack to 10° causes the pressure peak to increase and shift forward to about the 0.25 station along the 180° meridian, and to shift rearward to about the 0.70 station along the 0° meridian. At an angle of attack of 20°, the negative pressure peak is further increased and shifted away from the 0.50 station. Increasing the Mach number from 0.60 to 0.90 causes a decided increase in the negative pressure coefficients along the central portion of the body at all angles of attack.

Similar effects of Mach number and angle of attack noted for the fineness-ratio-3 body were also observed for the bodies of fineness ratio 5 and 6 (figs. 4(b) and 4(c)), except that the magnitude of the changes in pressure coefficient diminishes as the fineness ratio is increased.

Increasing the fineness ratio to 10, 15, and 20 causes a continued decrease in the effect of Mach number for constant angle of attack (figs. 4(d), 4(e), and 4(f)). At an angle of attack of 0°, the pressure coefficients are approaching zero. At angles of attack of 10° and 20°, the pressure gradients along both meridians of the bodies decrease with an increase in fineness ratio.

The same general trends of Mach number and angle of attack as observed for prolate spheroids of fineness ratio 10 and 15 are also observed for the parabolic body (fig. 5), except the changes in pressure coefficient near the nose are smaller as a result of the decreased bluntness of the nose.

Additional effects of nose bluntness are represented in figures 6 and 7. The ogive-cylinder body (fig. 6) has a nose shape that might be considered a sharpened version of a fineness-ratio-6 prolate-spheroid nose. This nose shape caused a reduction in pressure gradients near the nose, compared to the fineness-ratio-6 body. This was noted

Security Classification of This Report Has Been Cancelled

previously for the sharp-nose parabolic body. The minimum pressure and the effect of increasing Mach number from 0.60 to 0.90 were greater on the ogive-cylinder body. The effect of an increase in angle of attack was to displace the pressure distributions along both meridians and steepen the pressure gradients near the nose along the 0° meridian.

The bluntness of the hemispherical-nose body produced large pressure peaks that are associated with a spherical shape (fig. 7). These peaks occur at all Mach numbers and are somewhat ahead of the juncture of the hemispherical nose with the fineness-ratio-10 afterbody. The effect of increasing the Mach number from 0.30 to 0.60 is negligible, but further increasing the Mach number to 0.90 causes a decided increase in the negative pressure peak and produces a rearward movement of the low-pressure region, terminated by a shock located near the 0.25-body-length station. This effect was also noted for the fineness-ratio-3 prolate spheroid. With an increase in angle of attack to 10° and 20°, at a Mach number of 0.9, the pressure coefficients along the 180° meridian undergo a reduction in peak values compared to the zero angle-of-attack case and a rearward extension to the low-pressure region. Along the 0° meridian, the peak negative pressure coefficients are considerably lower than at an angle of attack of 0° at a Mach number of 0.3 but increase with an increase in Mach number.

Prediction of Incompressible Pressure Distribution

Along the 0° and 180° Meridians

Zero angle of attack.- Since the theoretical determination of compressible pressure distributions utilizes the incompressible theory, it is of interest to see how well the theory predicts low-speed pressure distributions. A comparison is made in figure 8 between several theoretical pressure distributions and low-speed experimental results for three prolate spheroids. At an angle of attack of 0° (fig. 8(a)), the classical potential theory (for example, refs. 8, 9, and 10) and the more recent method of reference 4 predict similar results along the entire lengths of the bodies of fineness ratio 6 and 10 but diverge near the forward and rear portions of the fineness-ratio-3 body. The theoretical pressure distributions are in excellent agreement with experimental results. At the rear part of the body, the sting may be influencing the pressures. The method of reference 10, however, agrees much better with experimental data than the method of reference 4.

Angles of attack.- The pressure distributions at angles of attack can be predicted either directly from incompressible theory (for example, ref. 10 or 4), or indirectly by adding to the zero angle-of-attack pressure distribution the increment in pressure coefficient due to angle of attack ΔP obtained from linearized theory (refs. 11, 12, and 13).

Security Classification of This Report Has Been Cancelled

At angles of attack of 10° and 20° (figs. 8(b) and 8(c)), theoretical pressure distributions obtained by the methods of references 4 and 10 and a combination of references 10 and 12 are compared with experimental results for the prolate spheroids of fineness ratio 3, 6, and 10. As in the zero angle-of-attack case, the three theoretical methods are almost the same along the central portion of the fineness-ratio-3 body and along the entire lengths of the bodies of fineness ratio 6 and 10.

Along the forward portion of the 0° meridian of the fineness-ratio-3 body, experimental pressure coefficients are in better agreement with the pressure coefficients predicted by either the method of reference 10 or the method of a combination of references 10 and 12 than the method of reference 4. Along the forward portion of the 180° meridian, the theories do not predict the shape of the pressure distribution, the negative pressure peak being more rearward than the theory predicts; however, the theory of reference 10 more nearly approaches the experimental results. This is probably due to exceeding the limitations of applicability of the theory.

For the bodies of fineness ratio 6 and 10, at angles of attack of 10° and 20° (figs. 8(b) and 8(c)), the three theoretical methods predict approximately the same pressure distribution and they are in excellent agreement with experimental pressure coefficients along the 0° meridian and along the forward portion of the 180° meridian. Along the rear portion of the 180° meridian, the theoretical and experimental pressure coefficients begin to diverge for the fineness-ratio-10 body at an angle of attack of 10°. This divergence becomes greater when the angle of attack is increased to 20°, where it also occurs on the fineness-ratio-6 body. The divergence between theory and experiment along the 180° meridian indicates that flow separation is occurring.

These comparisons indicate that, at a Mach number near zero, the method of reference 10 estimates the pressure distribution along the fineness-ratio-3 body at an angle of attack of 0° better than the method of reference 4 and that either method is satisfactory for the bodies of fineness ratio 6 or 10. At angles of attack, either the method of reference 10 or the combination of references 10 and 12 will predict the pressure coefficients along the 0° meridian of the fineness-ratio-3 body with a fair degree of accuracy. Along the 180° meridian, however, none of the three theories adequately predict the shape of the pressure distribution. For bodies of fineness ratio 6 or 10, the three methods will accurately predict the pressure distribution along the 0° or 180° meridians of the body, except where flow separation occurs.

Security Classification of This Report Has Been Cancelled

Prediction of Subsonic Pressure Distribution

Along the 0° and 180° Meridians

There are various methods available for computing the compressible pressure distribution on bodies of revolution. These methods utilize either the linearized form of the equations for compressible flow or corrections for the effects of Mach number applied to the incompressible pressure distribution itself. The former utilizes the Prandtl-Glauert correction applied to the incompressible-potential-flow equations. This method, as illustrated in reference 4, involves stretching the body in the free-stream direction, computing the induced-velocity component along the stretched body by potential-flow methods, and applying corrections to the induced velocities. The latter solution, which is relatively easy to compute, employs an exact calculation of the incompressible pressure distribution (refs. 8, 9, and 10) corrected to the desired Mach number by means of approximate correction formula. In the present paper, the latter method will be used.

Corrections for the effect of Mach number.- The incompressible pressure distributions obtained theoretically by the method of reference 10 (in fig. 8) for the prolate spheroids of fineness ratio 3, 6, and 10 have been transcribed into theoretical pressure distributions for a Mach number of 0.90 by using the slender-body and thick-body ratio corrections and the incremental corrections from figure 9 and the results are presented in figures 10(a), 10(b), and 10(c). The correction formulas are a simplification of the compressible-pressure-coefficient equations expressed as functions of Mach number and fineness ratio. The ratio-type corrections P_c/P_i, computed by six methods (refs. 4 and 14 to 16), are divided into slender-body and thick-body corrections. The slender-body corrections, consisting of four methods which are in close agreement with one another, are for use on bodies of fineness ratio 6 or greater (refs. 4 and 14 to 16). The thick-body corrections, consisting of two methods which approximately duplicate each other, are for use with thick bodies (refs. 4 and 15). The two groups give widely different correction factors for the fineness-ratio-3 body, but converge when the fineness ratio is increased.

The incremental-type correction $P_c - P_i$ (fig. 9) was computed by the method of reference 4 for the prolate spheroids of fineness ratio 3, 6, and 10 to provide an approximate compressible correction for an incompressible pressure distribution at angles of attack. This type of correction translates the whole pressure distribution in a negative direction.

The application of the correction formulas can be made by several methods of approach. The methods include: (1) the application of the correction formulas directly to the incompressible pressure distribution

Security Classification of This Report Has Been Cancelled

obtained theoretically at any angle of attack; (2) the use of the correction formulas with a combination of ΔP and zero angle-of-attack theory; and (3) the application of the correction formulas to the low-speed experimental results. (The values of ΔP are determined from cross-flow components and are considered independent of Mach number, provided the cross-flow velocity is small compared to the speed of sound. ΔP does not include viscous effects; see ref. 12.)

Correction formulas applied directly to incompressible pressure distributions.- The first method is presented in figures 10(a), 10(b), and 10(c), where the slender-body, the thick-body, and the $P_c - P_i$ corrections have been applied to the incompressible pressure distributions obtained theoretically for the prolate spheroids of fineness ratio 3, 6, and 10 at angles of attack of 0°, 10°, and 20°. At an angle of attack of 0° (fig. 10(a)), for the fineness-ratio-3 body, the agreement between the experimental pressure distribution and the pressure distribution predicted by the three correction methods is poor. For the bodies of fineness ratio 6 and 10, the three theoretical pressure distributions are in excellent agreement with experimental results along the central part of the body. Near the nose and tail, the theoretical pressure distributions, using the $P_c - P_i$ correction, diverge from the other two distributions and experiment. Near the tail, the sting is influencing the experimental pressures.

At an angle of attack of 10° (fig. 10(b)) for the fineness-ratio-3 body, the general agreement between theory and experiment is very poor, except along the forward portion of the 0° meridian where the theory, using the P_c/P_i correction, is in good agreement with experiment. For the bodies of fineness ratio 6 and 10, the $P_c - P_i$ correction gives the best over-all agreement with experimental results.

Increasing the angle of attack to 20° (fig. 10(c)) causes the theory and experiment to become more divergent for the fineness-ratio-3 body. For the bodies of fineness ratio 6 and 10, the theory, using the $P_c - P_i$ correction, is in excellent agreement with experiment all along the 0° meridian. The agreement between the theory and experiment along the 180° meridian is only fair near the nose and becomes increasingly poor toward the rear of the body because of flow separation, as was encountered in the incompressible case.

In general, figures 10(a), 10(b), and 10(c) show that, by using reference 10, along with either P_c/P_i correction, the pressure distribution at 0° angle of attack and Mach number 0.9 can be accurately predicted for slender bodies. For the thick body, the theoretical predictions are inadequate at an angle of attack of 0° and become more divergent with an increase in angle of attack, probably due to the body size and the

Security Classification of This Report Has Been Cancelled

fact that local velocities along most of the body are above sonic at a Mach number of 0.9. At angles of attack up to 20°, the theoretical pressure distribution, using the $P_c - P_i$ correction, accurately predicts the pressures along slender bodies, except where serious flow separation occurs.

Correction formulas applied to a combination of ΔP and zero angle-of-attack theory.- The prediction of compressible pressure distributions on bodies at angles of attack can be made by the second method. This method is the application of the correction formulas in conjunction with ΔP (ref. 12) and zero angle-of-attack incompressible theory (ref. 10). Pressure distributions predicted by this method, using each of the two forms of correction formulas (fig. 9), are presented in figures 10(d) and 10(e) for the prolate spheroids of fineness ratio 3, 6, and 10 at angles of attack of 10° and 20°. The two theoretical pressure distributions were obtained by correcting the incompressible zero angle-of-attack theory of reference 10 to a Mach number of 0.90 by P_c/P_i or $P_c - P_i$, then adding to it the increment for angle of attack ΔP (ref. 12).

At an angle of attack of 10°, for the fineness-ratio-3 prolate spheroid (fig. 10(d)), the pressure distributions computed by these methods do not agree with experimental results. For slender bodies of fineness ratio 6 and 10, either of the methods gives excellent agreement with experiment along the body except near the nose of the 180° meridian, where the theoretical method, using P_c/P_i, gives a better prediction. For an angle of attack of 20°, the disagreement between theory and experiment is greater. The two theoretical methods predict the pressures along the 0° meridian of the slender bodies to about the same accuracy. Along the 180° meridian, however, the agreement between theory and experiment is only fair near the nose and becomes increasingly poor toward the rear because of flow separation.

Correction formulas applied to low-speed experimental results.- The third method of predicting compressible pressure distributions along bodies of revolution is to use the correction formulas in conjunction with low-speed experimental results. The $P_c - P_i$ correction can be applied directly to low-speed experimental results at angles of attack, or the P_c/P_i correction can be applied to low-speed experimental results at an angle of attack of 0° and added to the experimental ΔP to form compressible pressure distributions at angles of attack. Pressure distributions predicted in this manner are presented in figures 10(f) and 10(g) for the prolate spheroids of fineness ratio 3, 6, and 10 at angles of attack of 10° and 20°. The pressure-distribution predictions at angles of attack of 10° and 20° for the fineness-ratio-3 body are in poor agreement with experimental results. For the bodies of fineness ratio 6 and 10, the predictions are in good agreement with experiment, even in the region of separated flow along the 180° meridian (figs. 10(f) and

Security Classification of This Report Has Been Cancelled

10(g)). The region of separated flow was present in the low-speed experimental results. These two applications of the correction formulas produced approximately the same pressure distribution. In general, especially where flow separation exists, pressure distributions at high subsonic speeds can be most accurately predicted by utilizing low-speed experimental results.

Prediction of Subsonic Pressure Distributions Around Prolate Spheroids

The incremental experimental pressure coefficients due to angle of attack ΔP used in figures 10(f) and 7(g) to predict pressure distributions along the 0° and 180° meridians of prolate spheroids were considered independent of Mach number (ref. 12). In figure 11, the experimental ΔP and its variation around the prolate spheroids of fineness ratio 5 and 10 at an angle of attack of 6° are compared with the theoretical ΔP (ref. 12) for the 0.1, 0.3, 0.6, and 0.9 stations, at Mach numbers from 0.30 to 0.90. For the fineness-ratio-5 body (fig. 11(a)), the agreement between theory and experiment is excellent for the 0.1, 0.3, and 0.6 stations. The 0.9 station is in the influence of the sting support and therefore is not expected to agree with theory. The same agreement between theory and experiment is noted for the fineness-ratio-10 body (fig. 11(b)). The close grouping of the test points for the various Mach numbers indicates that ΔP is essentially constant throughout the Mach number range presented here and that theory will predict ΔP around the body at low angles of attack.

Effect of Fineness Ratio and Angle of Attack on Separation

Since flow separation has been shown by the results presented in figures 8 and 10 to be the primary factor influencing the agreement of theory and experiment, it is of interest to examine the effect of fineness ratio and angle of attack on the location of separation. Theoretical and experimental pressure distributions are shown in figure 12 for the prolate spheroids of fineness ratio 6, 10, and 20 at angles of attack of 10°, 15°, and 20° and a Mach number of 0.9. The location of separation is assumed to be at that station where the positive pressure gradient of the theoretical pressure distribution becomes appreciably greater than that of the experimental pressure distribution. At an angle of attack of 10° there is no evidence of a separated region along the 180° meridian for the fineness-ratio-6 prolate spheroid. For the fineness-ratio-10 body, separation is beginning to occur around the 0.7 station. Increasing the fineness ratio to 20 causes the separated region to move forward to approximately the 0.1 station. At an angle of attack of 15°, separation

Security Classification of This Report Has Been Cancelled

exists possibly along the 180° meridian for the rear portion of the fineness-ratio-6 body, and this separated region shifts forward as the fineness ratio is increased. Increasing the angle of attack to 20° causes the separated region to move farther toward the nose for each of the bodies. This forward movement of the separated region with an increase in angle of attack is large for the thick body but decreases with an increase in fineness ratio because of the large separated region already present on the fineness-ratio-20 body.

Prediction of Transonic Pressure Distribution

Along the 0° and 180° Meridians

Zero angle of attack.- For Mach numbers near 1.0, no theories are available to predict the pressure distributions along bodies. The only practical manner of estimating the pressure distribution in this speed range is to extrapolate the incompressible theory to subsonic Mach numbers approaching 1.0 and to try to apply linear supersonic theories at low-supersonic Mach numbers near 1.0, as was done in reference 3. The theoretical distributions thus derived (same as ref. 3) are compared with experimental pressure distributions in figure 13 for a modified parabolic body at an angle of attack of 0°. The experimental data were obtained in the Langley 8-foot high-speed tunnel (ref. 1) and by the freely-falling-body technique (ref. 3).

At Mach numbers of 0.89 and 0.97 the experimental data are in good agreement with the pressures predicted by the subsonic theory. (Near the tail of this body pressures measured in the 8-foot high-speed tunnel exhibit some influence of the sting mount.) Increasing the Mach number to 1.02 causes a more pronounced change in the shape of the pressure distribution, a peak being developed over the rear part of the body. The level of the free-flight data may be in error because of a possible error in the measurement of the reference pressure as reported in reference 3. The measured data at a Mach number of 1.02 were compared with theoretical distributions at a Mach number of 1.05 and good agreement was obtained. Increasing the Mach number to 1.11 does not appreciably change the shape of the distribution and theory and experiment remain in good agreement.

Angles of attack.- Similar data for the modified parabolic body at an angle of attack of 20° are shown in figure 14. The theoretical distributions presented in this figure are the zero angle-of-attack distributions in figure 13, plus an increment in pressure coefficient for the angle-of-attack effect ΔP (ref. 12). The experimental data are from the Langley 8-foot high-speed tunnel (ref. 1).

Security Classification of This Report Has Been Cancelled

At a Mach number of 0.97 the agreement between theory and experiment is similar to that previously shown in figures 10 and 12 for a slender prolate spheroid in which separation prevents the expected pressure recovery along the 180° meridian. Increasing the Mach number to 0.99, 1.02, and 1.11 causes only gradual and minor changes in the shape of the pressure distribution and a slight decrease in the pressures near the rear portion of the body. At Mach numbers of 1.02 and 1.11 the theoretical and experimental pressure distributions are in agreement along the 0° meridian, except at the rear, and in disagreement along the 180° meridian. The results of these comparisons between theory and experiment show the same effects of separation in producing disagreements as observed at subsonic speeds (figs. 8, 10, and 12).

Experimental values of ΔP were evaluated by utilizing data for angles of attack of 0° and 20° at a Mach number of 0.79 (from ref. 1). These experimental values of ΔP were then added to the theoretical zero angle-of-attack pressure distributions of figure 13 to define the pressure-distribution predictions at an angle of attack of 20° which include the effects of flow separation (fig. 14). For each transonic Mach number, the pressure distributions obtained by this method are in excellent agreement with the experimental pressures along the 0° meridian. This method also satisfactorily predicts the pressure distribution along the 180° meridian of the body in the region of separated flow.

Prediction of Subsonic and Transonic Circumferential Pressure Distributions Around the Modified Parabolic Body

The incremental pressure coefficients due to angle of attack ΔP and their variations around the modified parabolic body at an angle of attack of 12° are presented in figure 15. The upper plot in figure 15 is for the 46-percent station, which is also representative of flow conditions forward of this station. The experimental values of ΔP were obtained from references 1 and 2 at Mach numbers of 0.6, 0.9, 0.99, and 1.13 and are compared with the theoretical variation of ΔP around the body (ref. 12). The agreement between theory and experiment is very good.

The lower plot in figure 15 is for the 70-percent station on the body and is representative of conditions around the body where flow separation exists. The disagreement between theory and experiment indicates an appreciable extent of separation along the 180° meridian. The effects of separation extend around the sides of the body beyond the 90° meridian. These data indicate that the theory reasonably estimates the incremental pressures around this body except where flow separation occurs.

Security Classification of This Report Has Been Cancelled

The close grouping of the test points for the various Mach numbers indicates there is no change in the flow characteristics through the transonic speed range and that the experimental value of ΔP at any station around the body remains essentially constant through the subsonic and transonic Mach number ranges. Low-speed pressure measurements on the body at the desired angle of attack can therefore be used to predict the pressure distribution at the corresponding position on the body at transonic speeds, even in the region of separated flow.

CONCLUSIONS

A comparison of experimental pressure distributions and theoretical pressure distributions computed by various methods for prolate spheroids of fineness ratio from 3 to 20 at Mach numbers from 0.3 to 0.9 and for a slender body of fineness ratio 12 at Mach numbers from 0.6 to 1.13 indicated the following conclusions:

1. At an angle of attack of 0° and over the bottom of the body at other angles of attack, the pressure distributions may be adequately predicted at subsonic and transonic speeds by the use of available theories.

2. For conditions where flow separation exists, pressure distributions at high-subsonic and transonic speeds can be predicted with fair accuracy by utilizing low-speed experimental results.

3. Separation of the flow occurs over the top side of the body at angles of attack, and the location of separation moves forward as either the angle of attack or the fineness ratio is increased.

Langley Aeronautical Laboratory
National Advisory Committee for Aeronautics
Langley Field, Va.

Security Classification of This Report Has Been Cancelled

REFERENCES

1. Loving, Donald L., and Williams, Claude V.: Basic Pressure Measurements on a Fuselage and a 45° Sweptback Wing-Fuselage Combination at Transonic Speeds in the Slotted Test Section of the Langley 8-Foot High-Speed Tunnel. NACA RM L51F05, 1951.

2. Loving, Donald L., and Estabrooks, Bruce B.: Transonic-Wing Investigation in the Langley 8-Foot High-Speed Tunnel at High Subsonic Mach Numbers and at a Mach Number of 1.2. Analysis of Pressure Distribution of Wing-Fuselage Configuration Having a Wing of 45° Sweepback, Aspect Ratio 4, Taper Ratio 0.6, and NACA 65A006 Airfoil Section. NACA RM L51F07, 1951.

3. Thompson, Jim Rogers: Measurements of the Drag and Pressure Distribution on a Body of Revolution Throughout Transition From Subsonic to Supersonic Speeds. NACA RM L9J27, 1950.

4. Matthews, Clarence W.: A Comparison of the Experimental Subsonic Pressure Distributions About Several Bodies of Revolution With Pressure Distributions Computed by Means of the Linearized Theory. NACA TN 2519, 1952. (Supersedes NACA RM L9F28.)

5. Wright, Ray H., and Ward, Vernon G.: NACA Transonic Wind-Tunnel Test Sections. NACA RM L8J06, 1948.

6. Stack, John, Lindsey, W. F., and Littell, Robert E.: The Compressibility Burble and the Effect of Compressibility on Pressures and Forces Acting on an Airfoil. NACA Rep. 646, 1938.

7. Herriot, John G.: Blockage Corrections for Three-Dimensional-Flow Closed-Throat Wind Tunnels, With Consideration of the Effect of Compressibility. NACA Rep. 995, 1950. (Supersedes NACA RM A7B28.)

8. Lamb, Horace: Hydrodynamics. Fourth ed., Cambridge Univ. Press, 1916.

9. Munk, Max M.: Fluid Mechanics, Pt. II. Ellipsoids of Revolution. Vol. I of Aerodynamic Theory, div. C, ch. VII, secs. 2 to 9, W. F. Durand, ed., Julius Springer (Berlin), 1934, pp. 277-288.

10. Zahm, A. F.: Flow and Drag Formulas for Simple Quadrics. NACA Rep. 253, 1927.

11. Tsien, Hsue-Shen: Supersonic Flow Over an Inclined Body of Revolution. Jour. Aero. Sci., vol. 5, no. 12, Oct. 1938, pp. 480-483.

Security Classification of This Report Has Been Cancelled

12. Allen, H. Julian: Pressure Distribution and Some Effects of Viscosity on Slender Inclined Bodies of Revolution. NACA TN 2044, 1950.

13. Lighthill, M. J.: Supersonic Flow Past Bodies of Revolution. R. & M. No. 2003, British A.R.C., 1945.

14. Schmieden, C., and Kawalki, K. H.: Contribution to the Problem of Flow at High Speed. NACA TM 1233, 1949.

15. Herriot, John G.: The Linear Perturbation Theory of Axially Symmetric Compressible Flow With Application to the Effect of Compressibility on the Pressure Coefficient at the Surface of a Body of Revolution. NACA RM A6H19, 1947.

16. Lees, Lester: A Discussion of the Application of the Prandtl-Glauert Method to Subsonic Compressible Flow Over a Slender Body of Revolution. NACA TN 1127, 1946.

Security Classification of This Report Has Been Cancelled

TABLE I.- ORDINATES OF THE HEMISPHERICAL-NOSE, OGIVE-CYLINDER, PARABOLIC, AND MODIFIED PARABOLIC BODIES

Hemispherical-nose		Ogive-cylinder		Parabolic (RM-10)		Modified parabolic	
x/l, percent	r/l, percent	x/l, percent	r/l, percent	x/l, percent	r/l, percent	x/l, percent	r/l, percent
0	0	0	0	0	0	0	0
.455	2.836	1.11	.366	1.00	.132	.50	.231
.909	3.964	2.22	.722	2.00	.262	.75	.298
1.364	4.782	3.33	1.067	4.00	.516	1.25	.428
1.818	5.455	4.44	1.400	6.00	.761	2.50	.722
3.636	7.273	5.56	1.711	8.00	.997	5.00	1.205
5.454	8.327	8.33	2.333	10.00	1.225	7.50	1.613
7.273	8.909	11.11	3.100	15.00	1.756	10.00	1.971
9.091	9.091	13.33	3.567	20.00	2.233	15.00	2.593
18.182	9.055	15.56	3.978	25.00	2.655	20.00	3.090
27.270	8.909	17.78	4.344	30.00	3.023	25.00	3.465
36.364	8.673	20.00	4.800	40.00	3.597	30.00	3.741
45.455	8.327	22.20	4.933	50.00	3.954	35.00	3.932
54.545	7.873	27.78	5.389	60.00	4.093	40.00	4.063
63.636	7.273	33.33	5.556	61.40	4.096	45.00	4.142
72.727	6.491	50.00	5.556	70.00	3.999	50.00	4.167
81.818	5.455	75.00	5.556	80.00	3.691	55.00	4.129
90.910	3.964	100.00	5.556	90.00	3.137	60.00	4.023
100.000	0			100.00	2.487	65.00	3.842
						70.00	3.562
						75.00	3.128
						80.00	2.526
						85.00	1.852
						90.00	1.125
						95.00	.438
						100.00	0

NACA

Security Classification of This Report Has Been Cancelled

CONFIDENTIAL

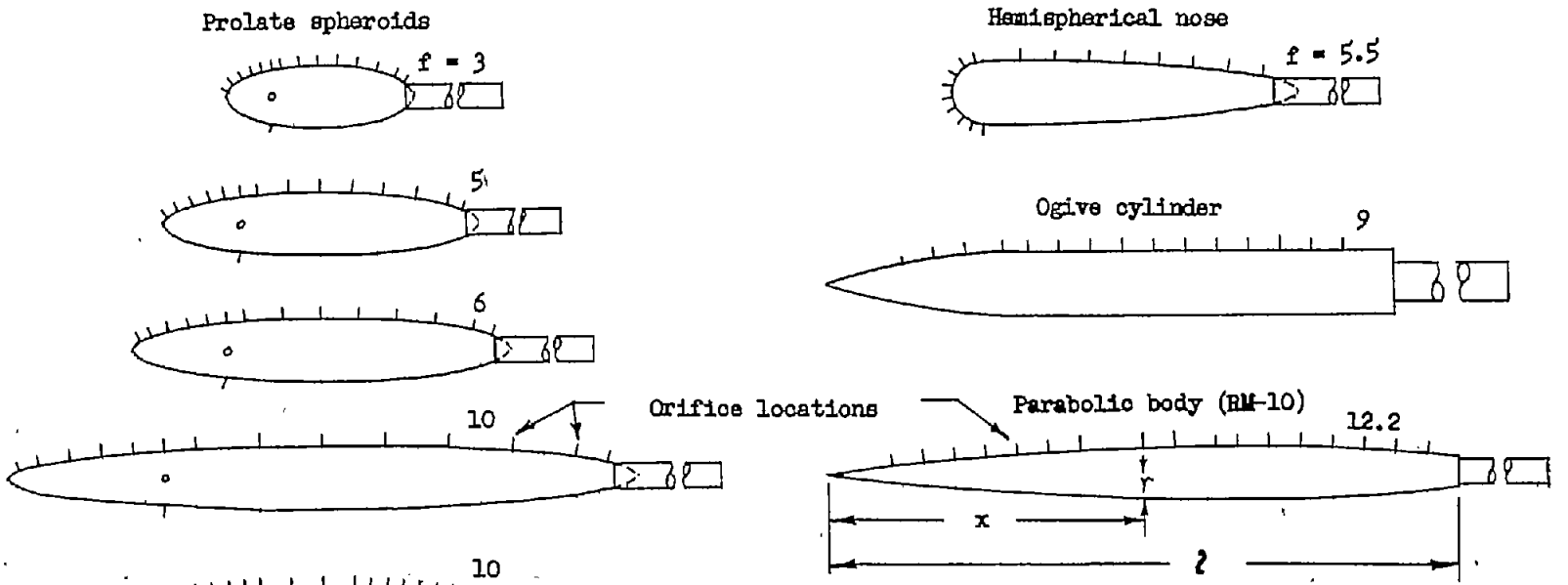

Profiles	f	Length (in.)	Diameter (in.)	Sting diameter (in.)
Prolate spheroids	3	3	1.000	0.375
	5	5	1.000	.375
	6	6	1.000	.375
	10	10	1	.375
	10	5	.5	.250
	15	7.5	.5	.25
	20	10.	.5	.25
Hemispherical nose	5.5	5.5	1.0	.375
Ogive cylinder	9	9	1	.600
Parabolic (RM-10)	12.2	10	.833	.375

Figure 1.- Profiles and orifice locations of bodies tested.

CONFIDENTIAL

Security Classification of This Report Has Been Cancelled

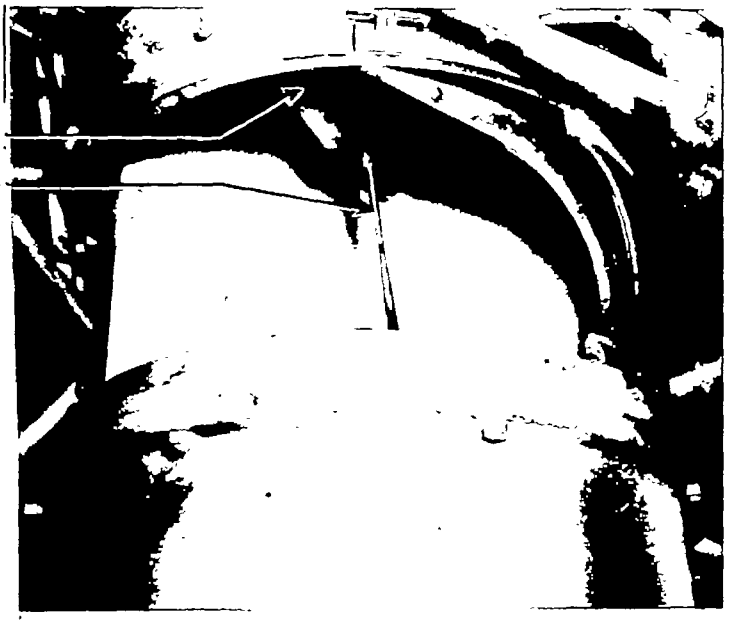

(a) Body installation.

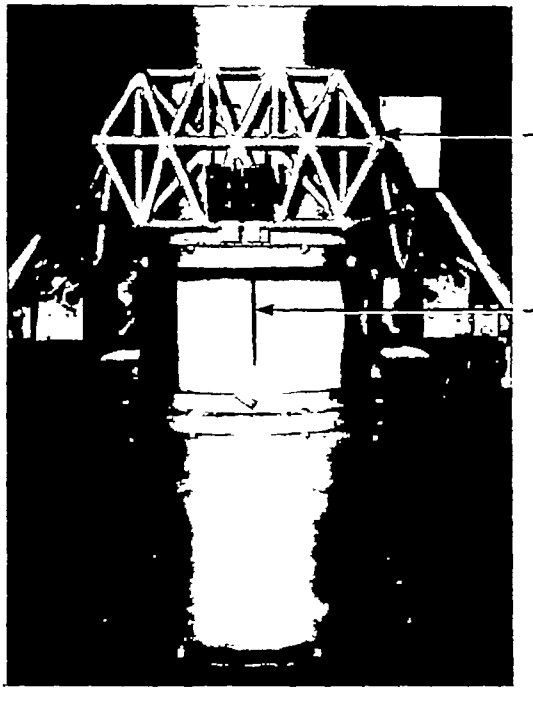

NACA
L-75090

(b) Tunnel configuration.

Figure 2.- Langley 24-inch high-speed tunnel test section showing the fineness-ratio-20 prolate spheroid at $\alpha = 10^{\circ}$.

Security Classification of This Report Has Been Cancelled

CONFIDENTIAL

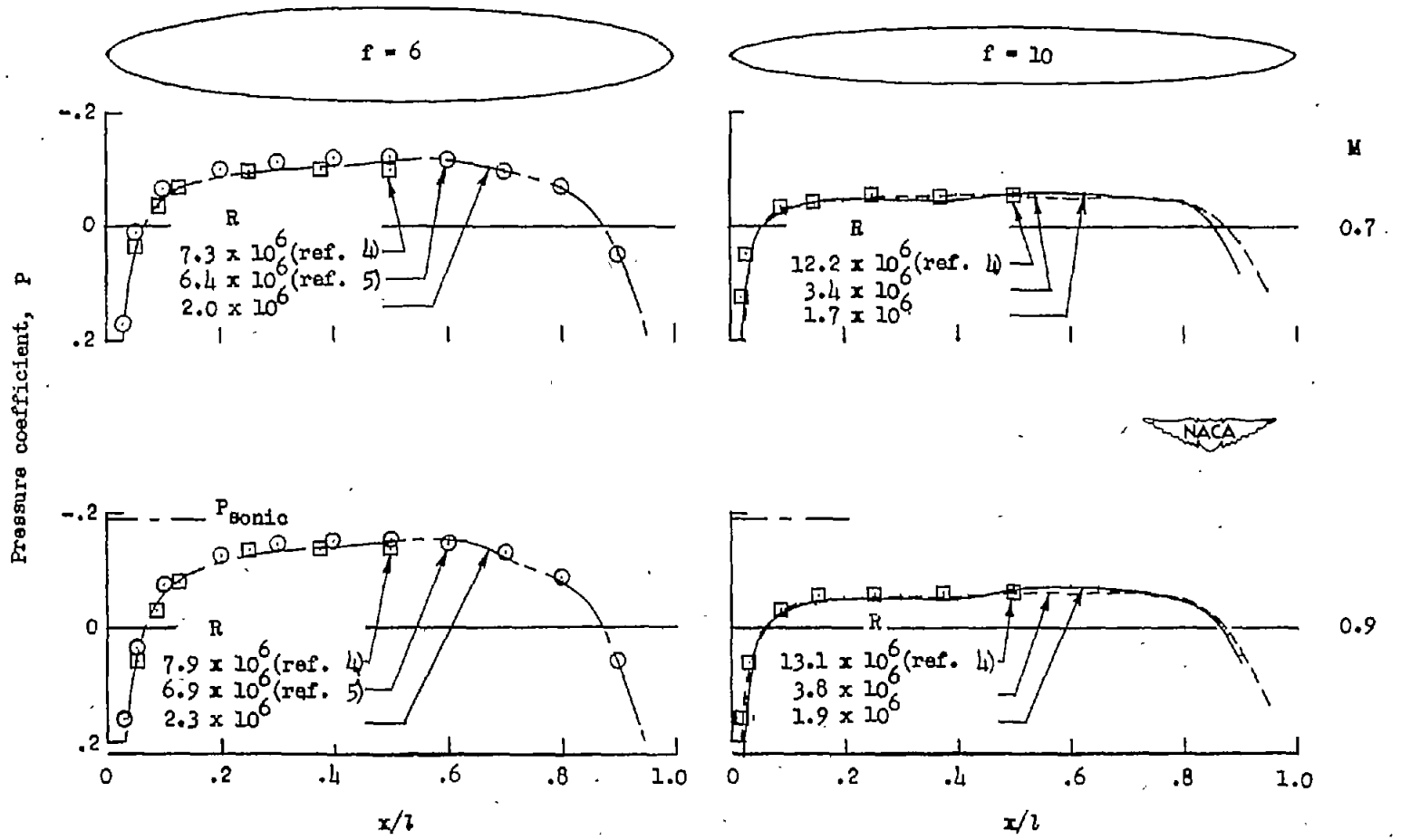

(a) $\alpha = 0^{\circ}$.

Figure 3.- Effects of change in Reynolds number on the pressure distribution along prolate spheroids.

CONFIDENTIAL

Security Classification of This Report Has Been Cancelled

CONFIDENTIAL

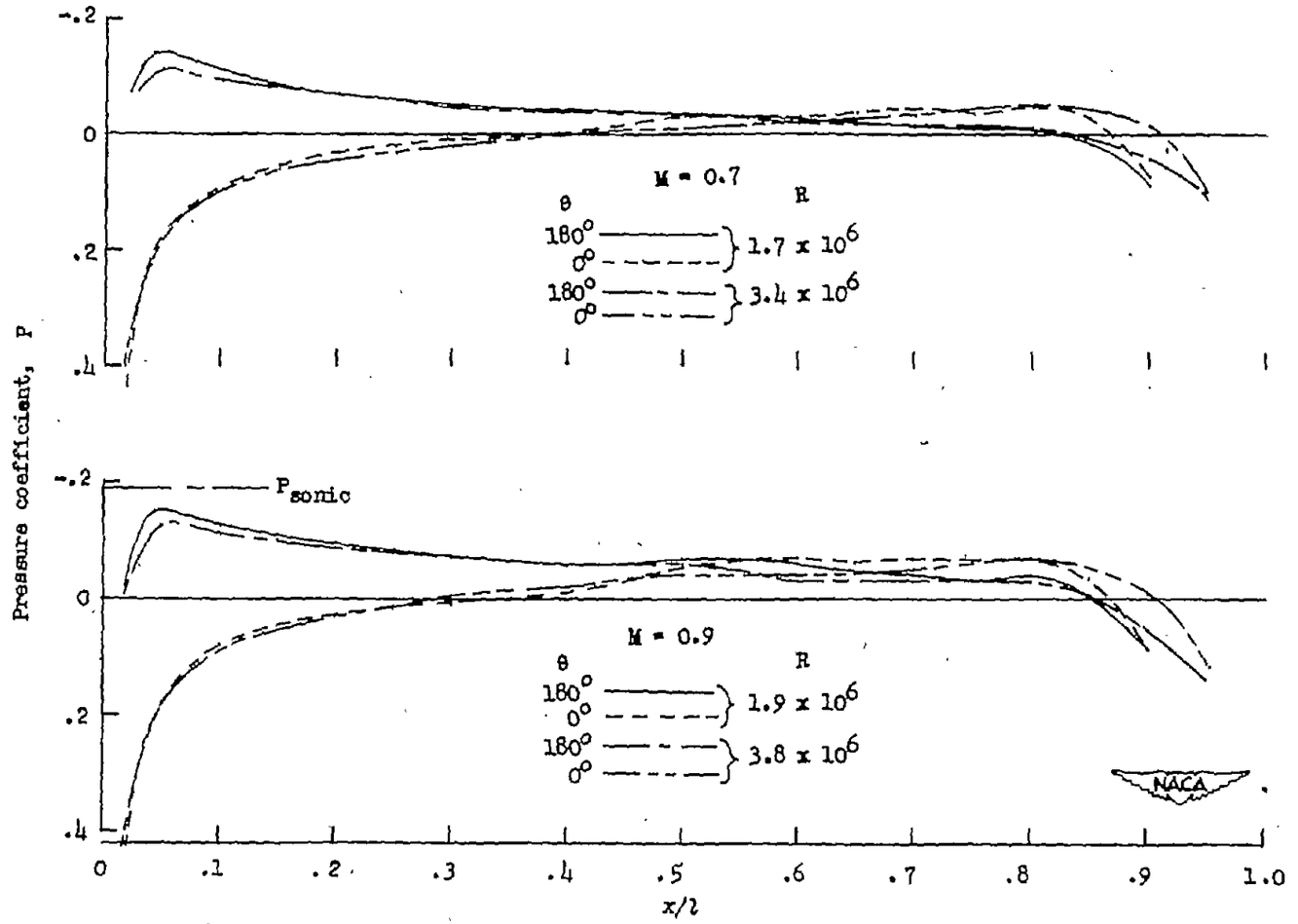

(b) $\alpha = 10^{\circ}$.

Figure 3.- Concluded.

CONFIDENTIAL

Security Classification of This Report Has Been Cancelled

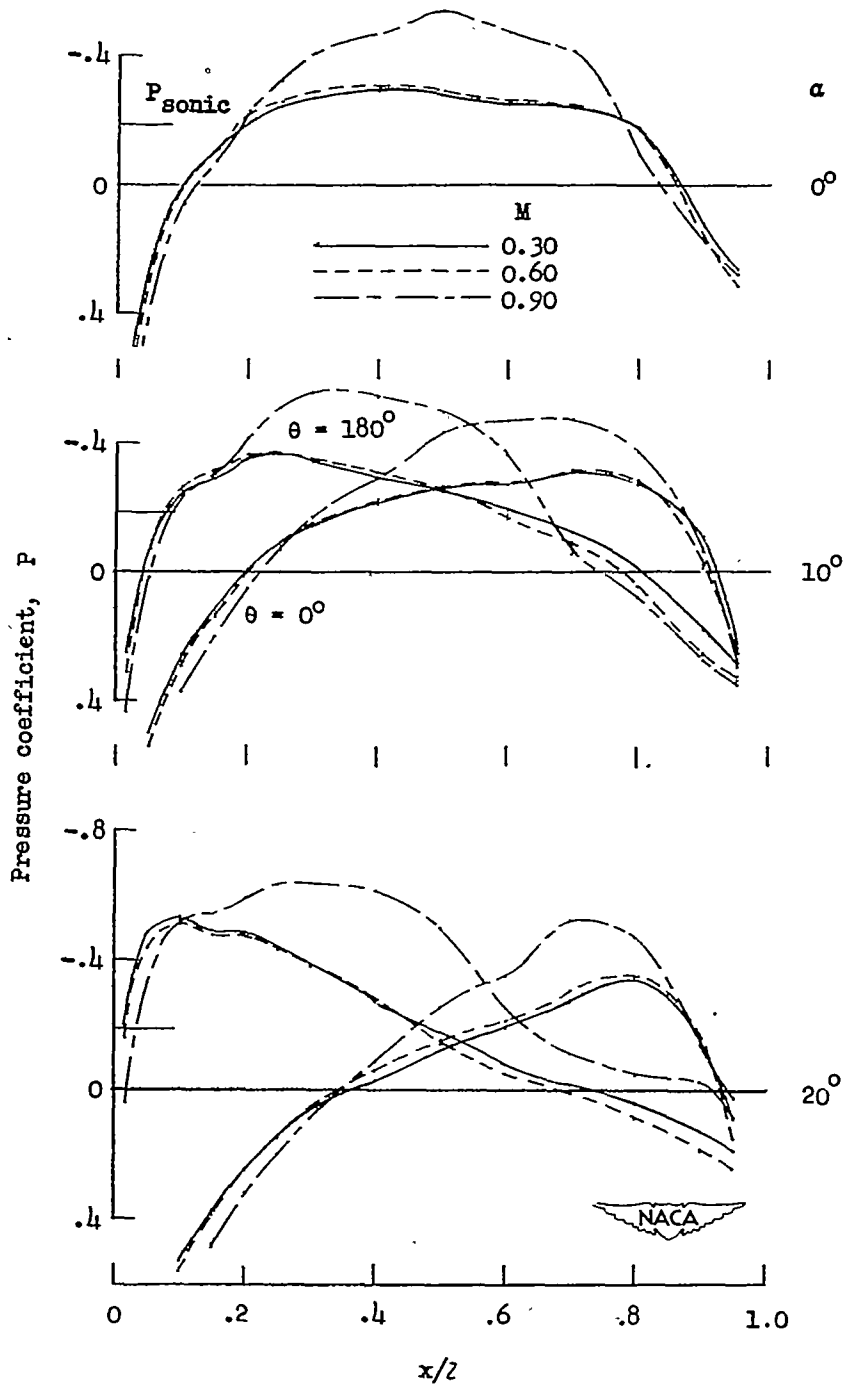

(a) f = 3.

Figure 4.- Effect of Mach number and angle of attack on pressure distributions along prolate spheroids (P_{sonic} for M = 0.9).

Security Classification of This Report Has Been Cancelled

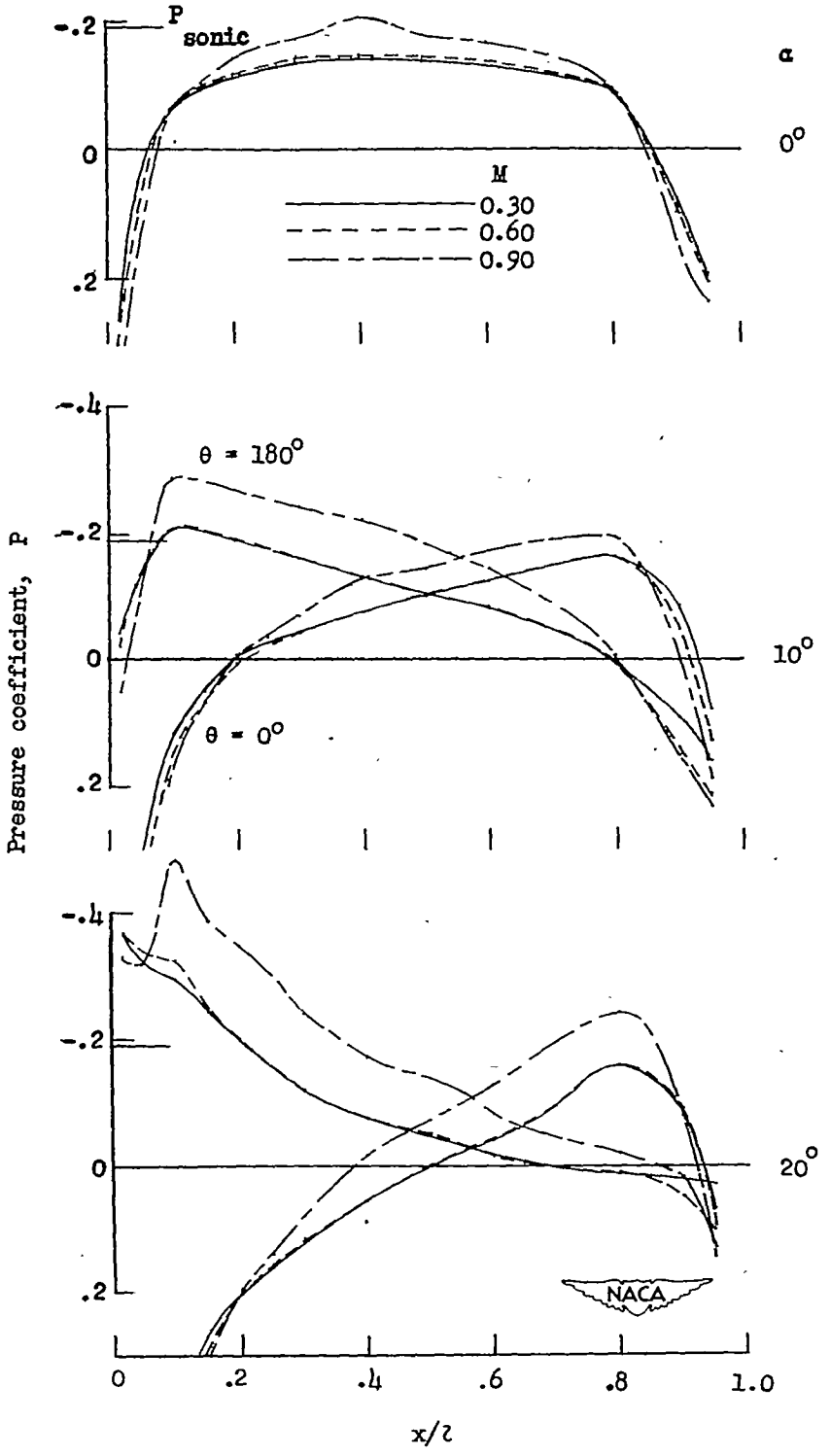

(b) f = 5.

Figure 4.- Continued.

Security Classification of This Report Has Been Cancelled

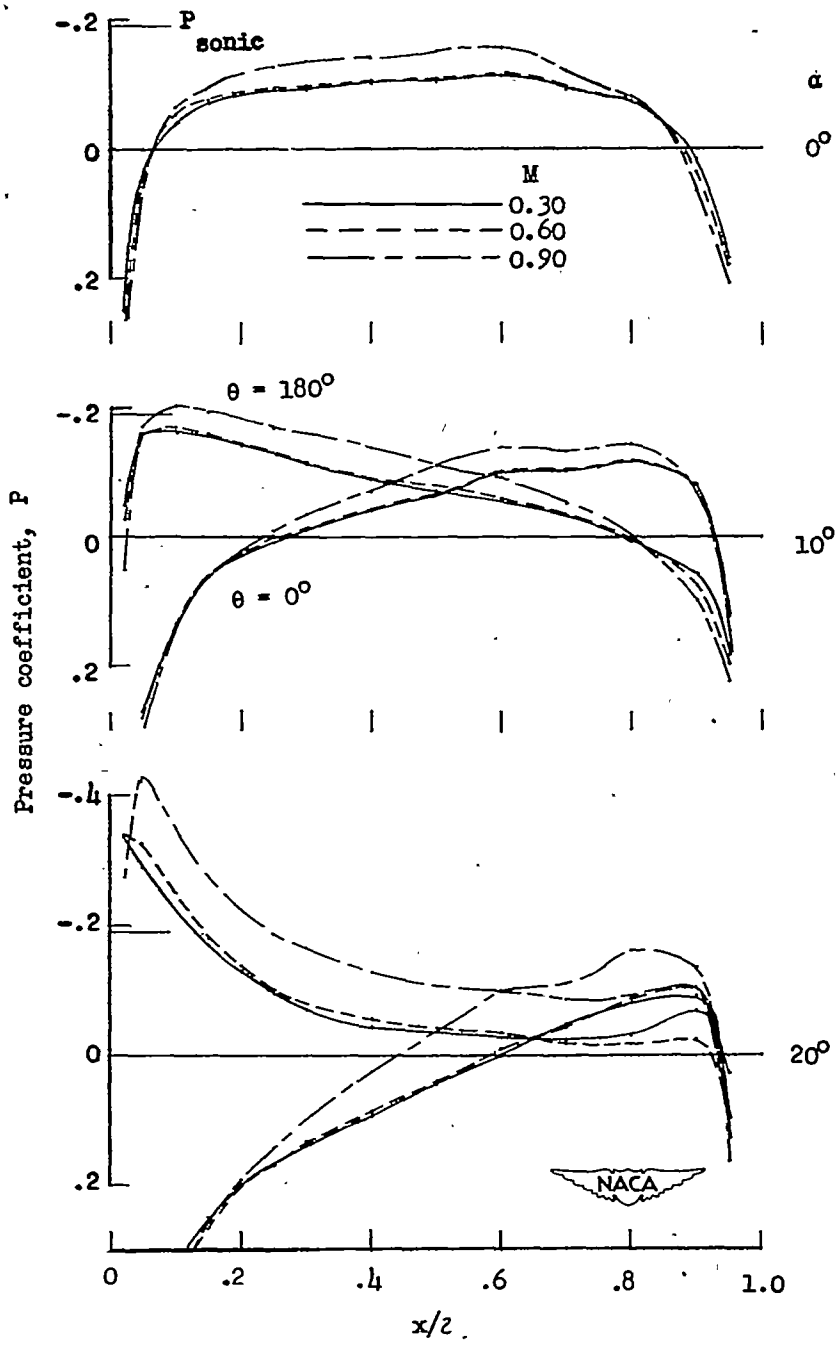

(c) f = 6.

Figure 4.- Continued.

Security Classification of This Report Has Been Cancelled

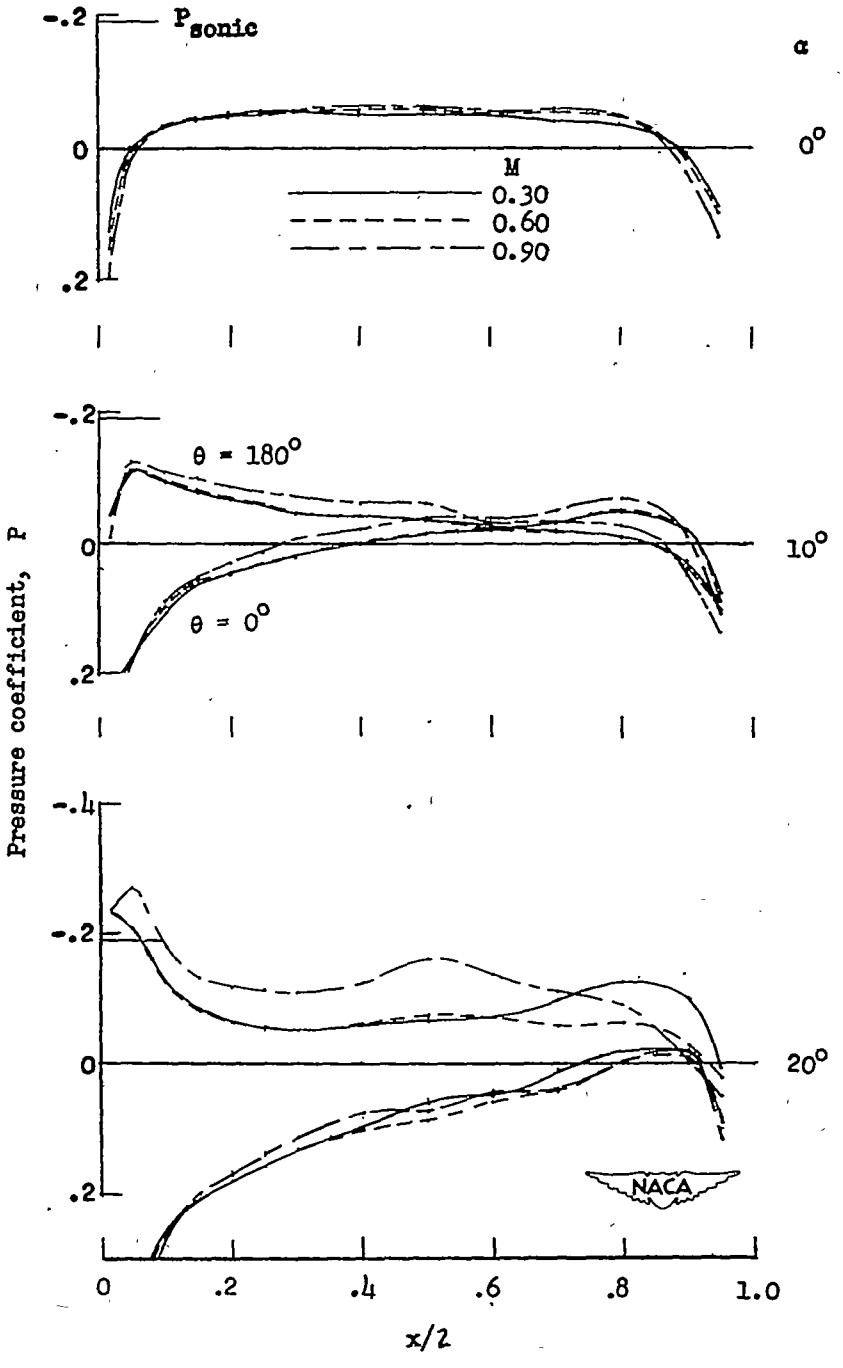

(d) f = 10.

Figure 4.- Continued.

Security Classification of This Report Has Been Cancelled

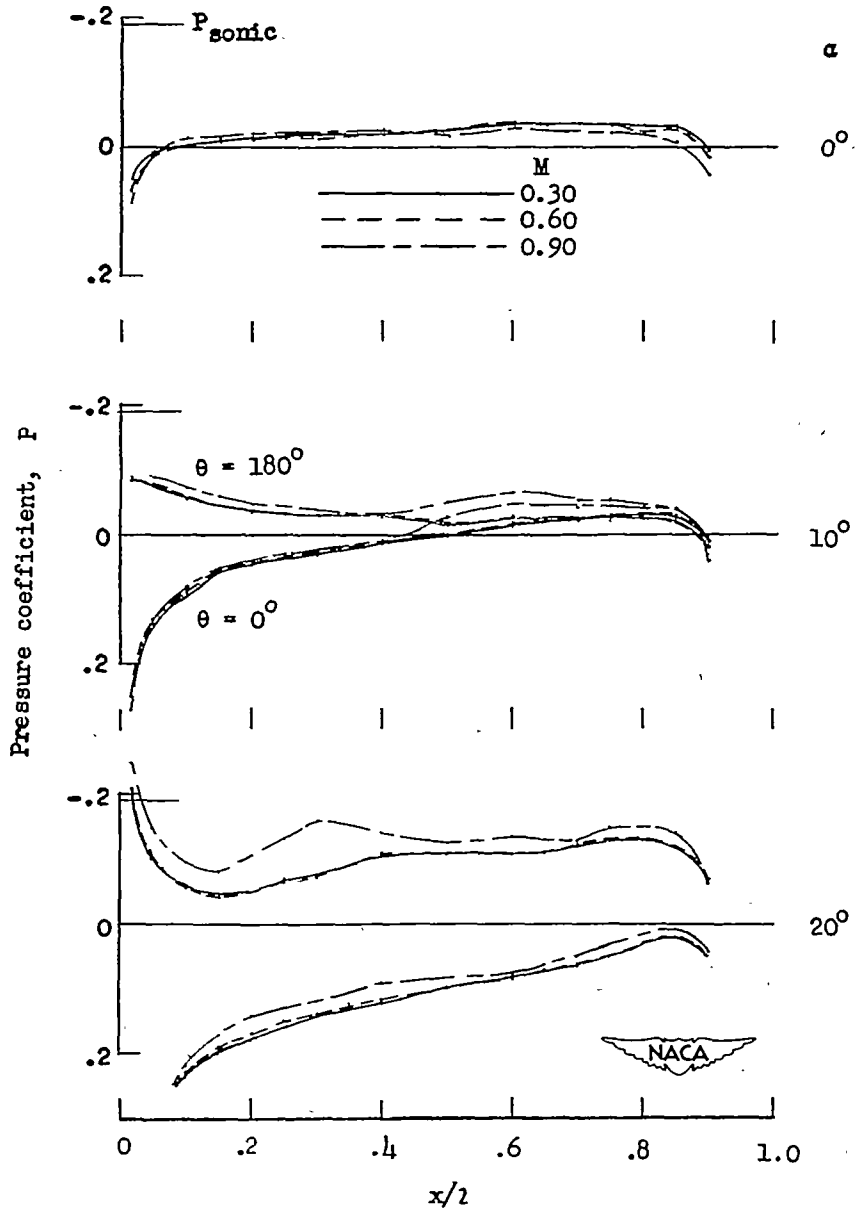

(e) f = 15.

Figure 4.- Continued.

Security Classification of This Report Has Been Cancelled

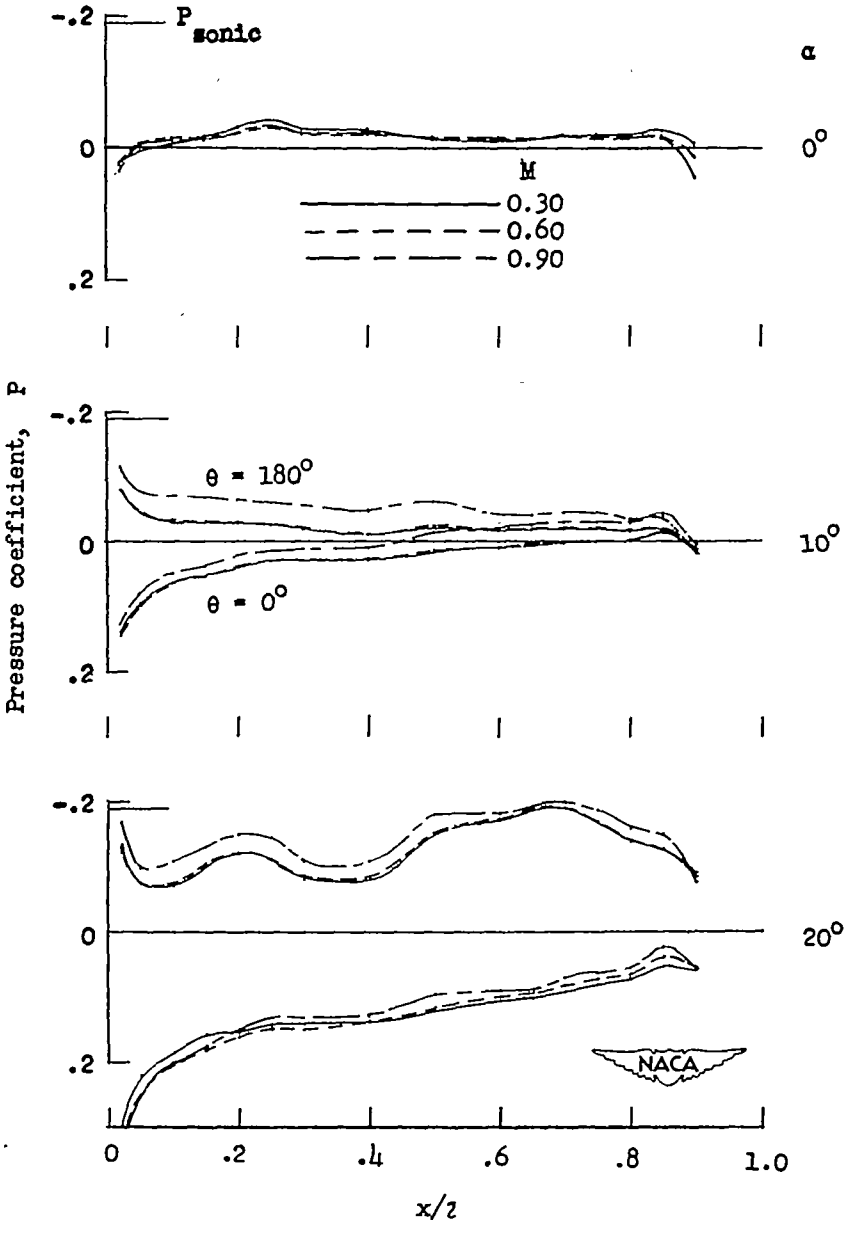

(f) f = 20.

Figure 4.- Concluded.

Security Classification of This Report Has Been Cancelled

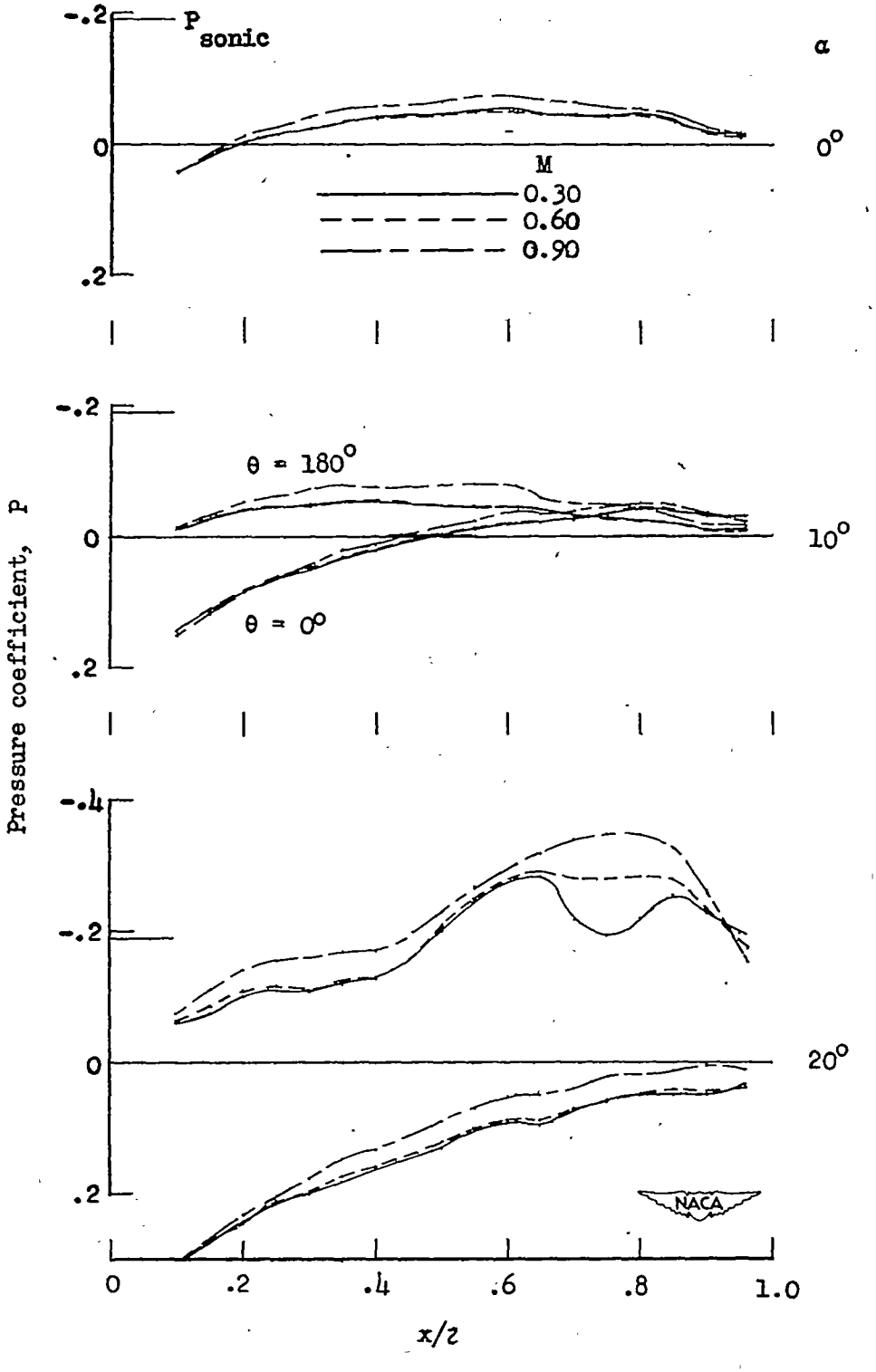

Figure 5.- Effect of Mach number and angle of attack on the pressure distribution along the parabolic body $\left(P_{sonic}\right.$ for $\left.M = 0.9\right)$. $f = 12.2$.

Security Classification of This Report Has Been Cancelled

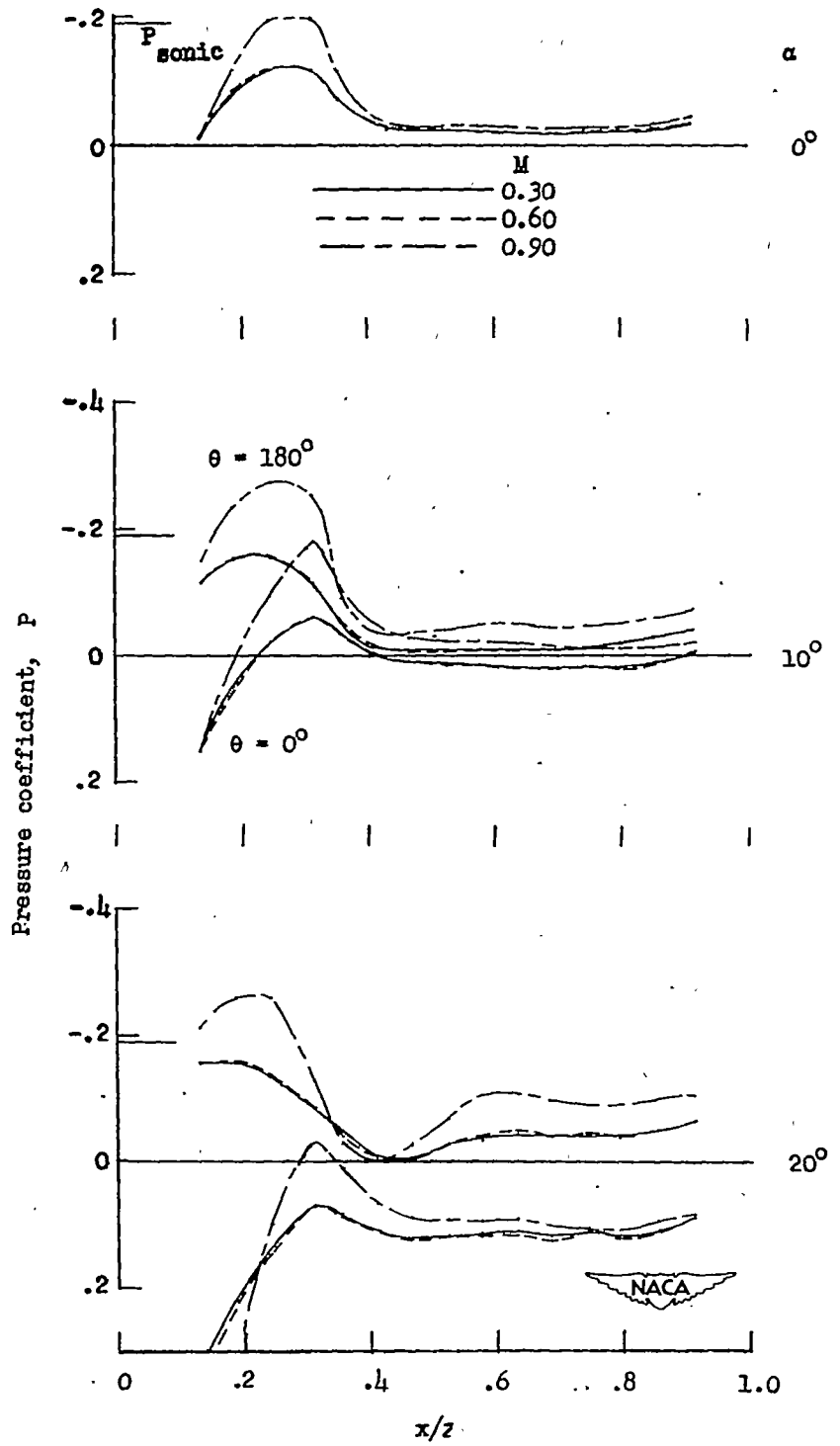

Figure 6.- Effect of Mach number and angle of attack on the pressure distribution along the ogive-cylinder body $\left(P_{sonic}\right.$ for $\left.M = 0.9\right)$. $f = 9$.

Security Classification of This Report Has Been Cancelled

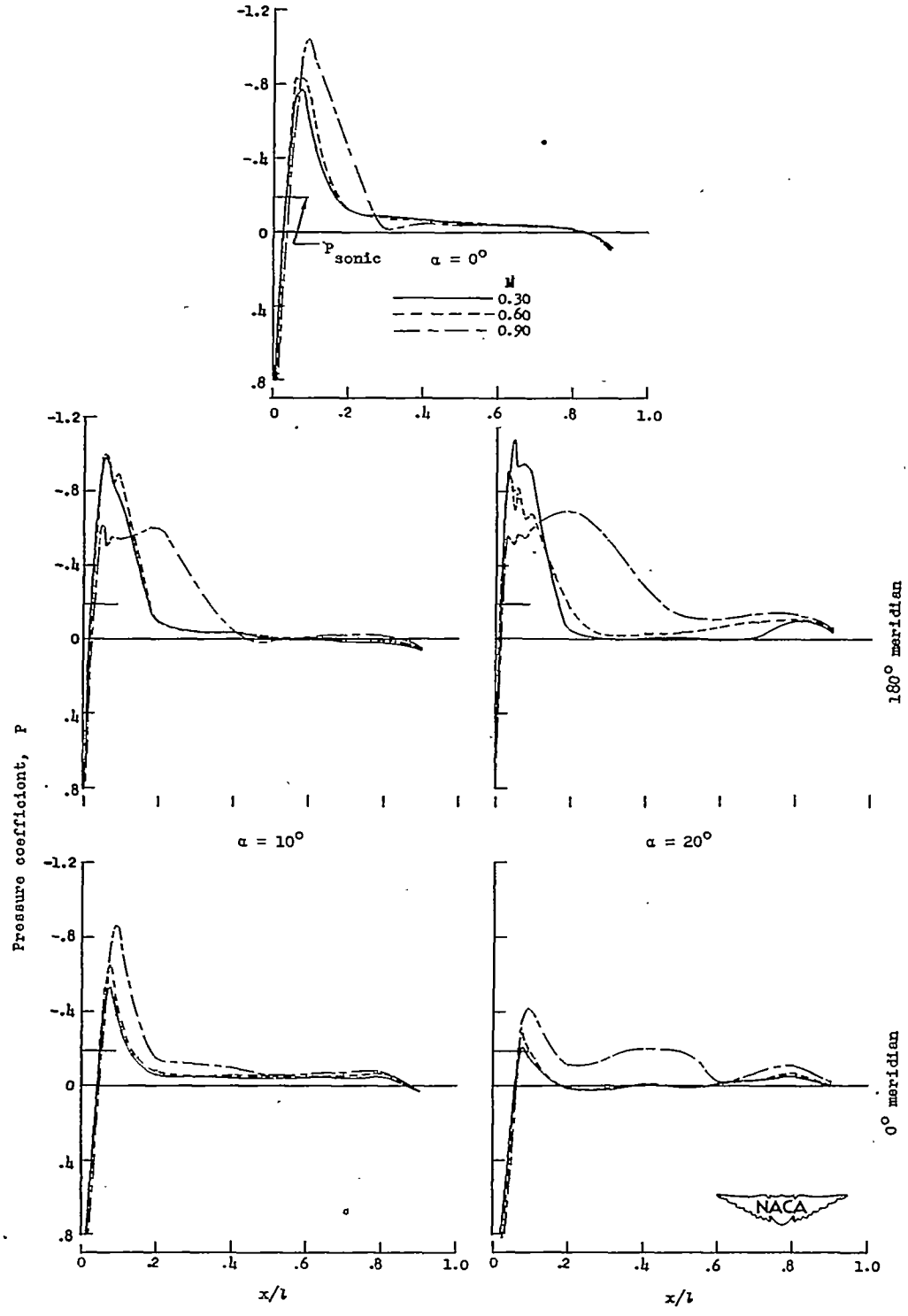

Figure 7.- Effect of Mach number and angle of attack on the pressure distribution along the hemispherical-nose body $\left(P_{sonic}\right.$ for $\left.M = 0.9\right)$. $f = 5.5$.

Security Classification of This Report Has Been Cancelled

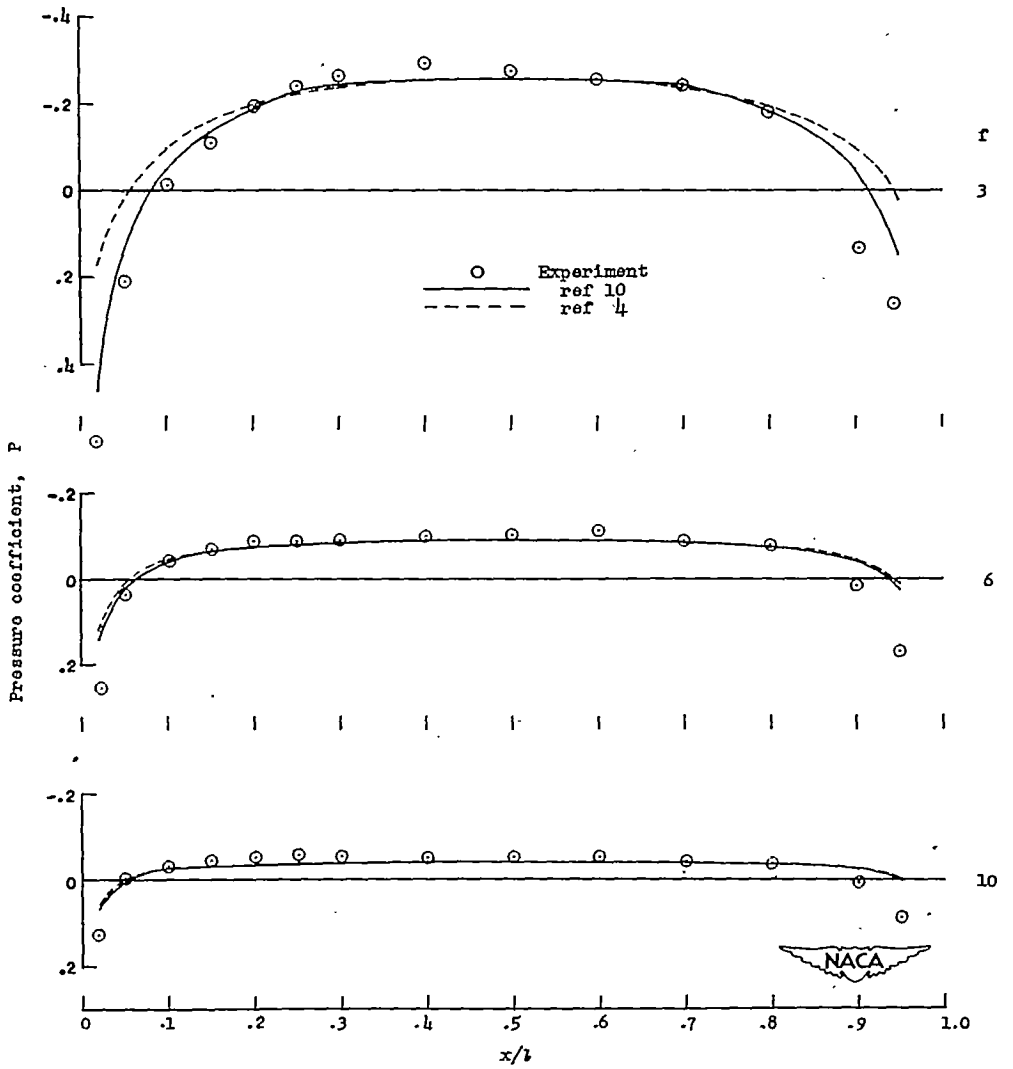

(a) $\alpha = 0^{\circ}$.

Figure 8.- Comparison of incompressible theoretical and experimental pressure distributions over the 0° and 180° meridians of several prolate spheroids.

Security Classification of This Report Has Been Cancelled

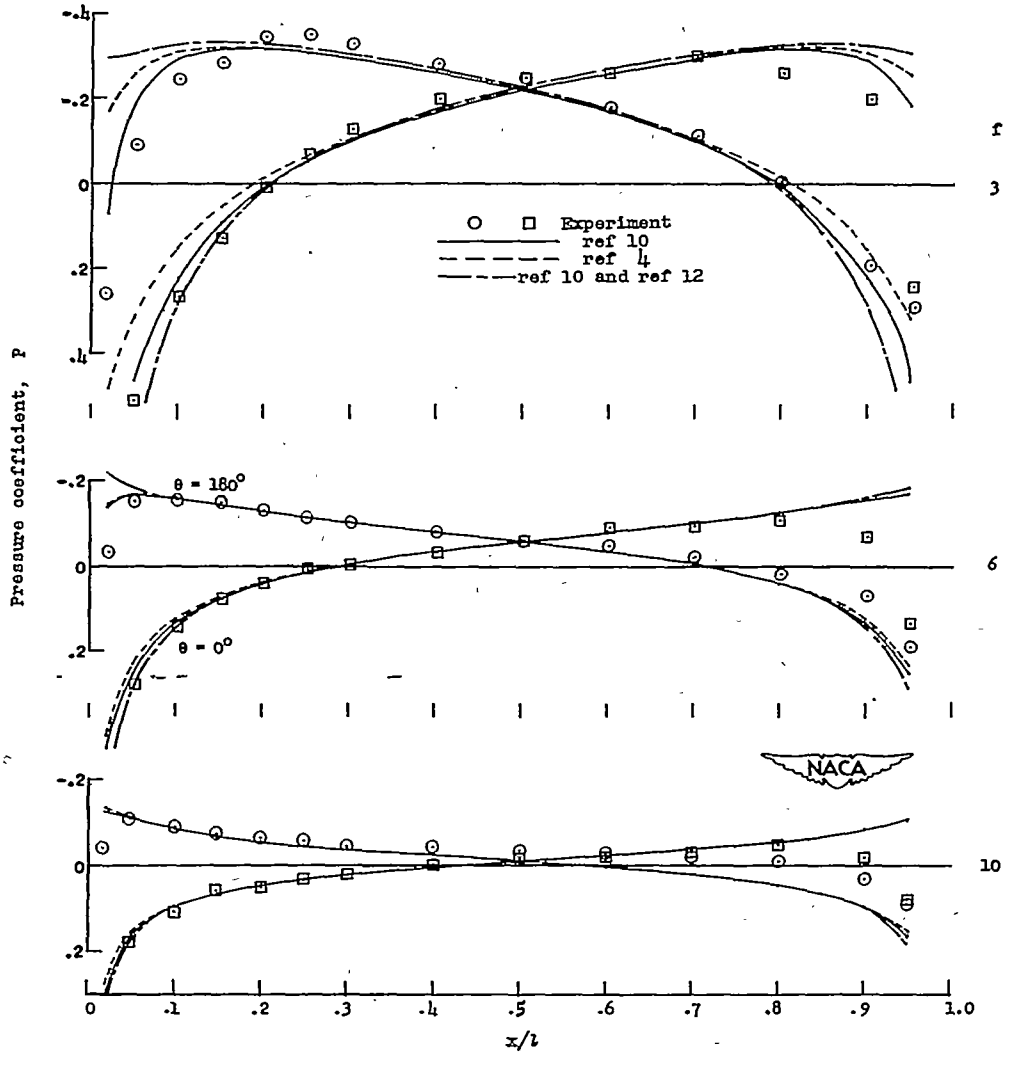

(b) $\alpha = 10^{\circ}$.

Figure 8.- Continued.

Security Classification of This Report Has Been Cancelled

5X

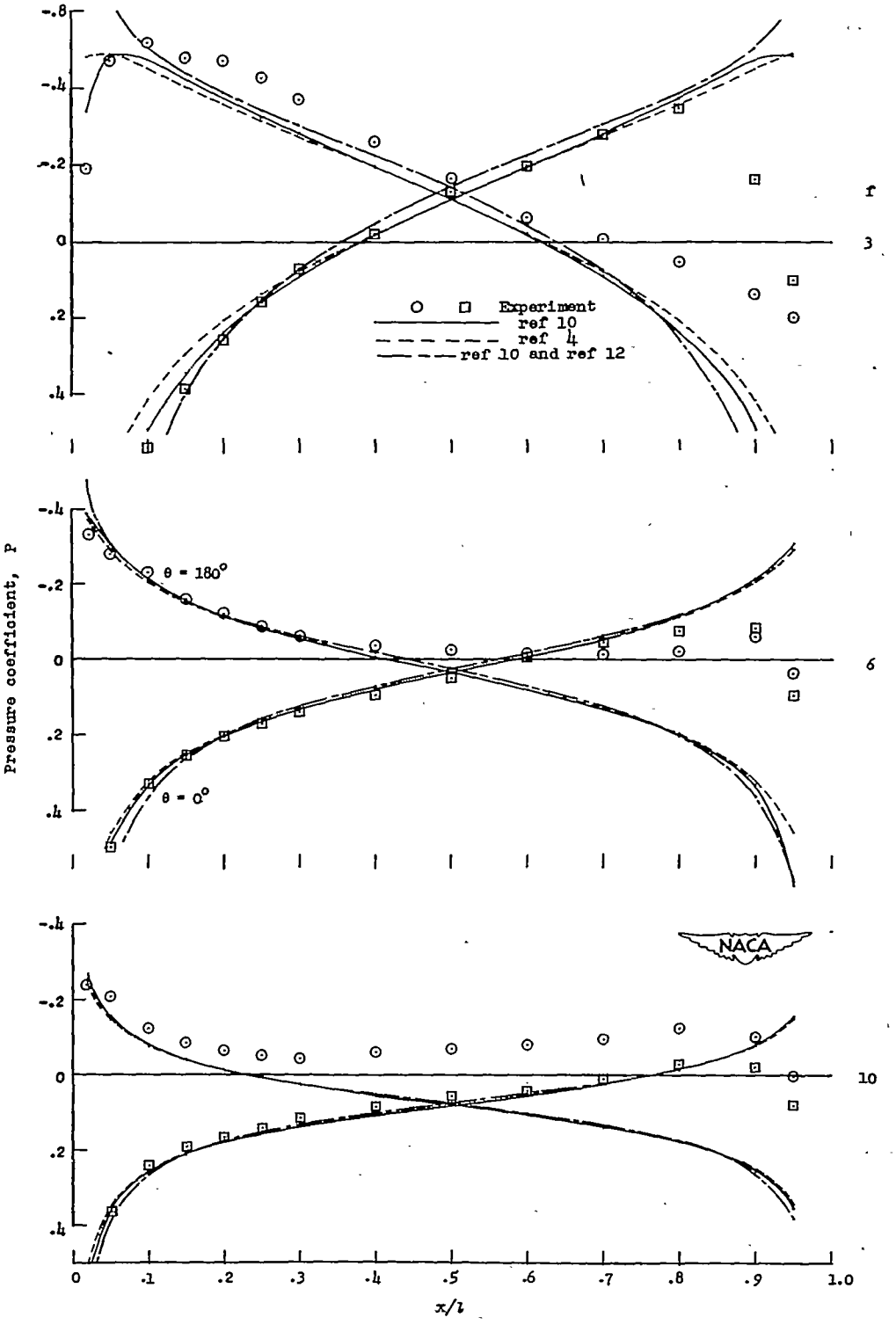

(c) $\alpha = 20^{\circ}$.

Figure 8.- Concluded.

Security Classification of This Report Has Been Cancelled

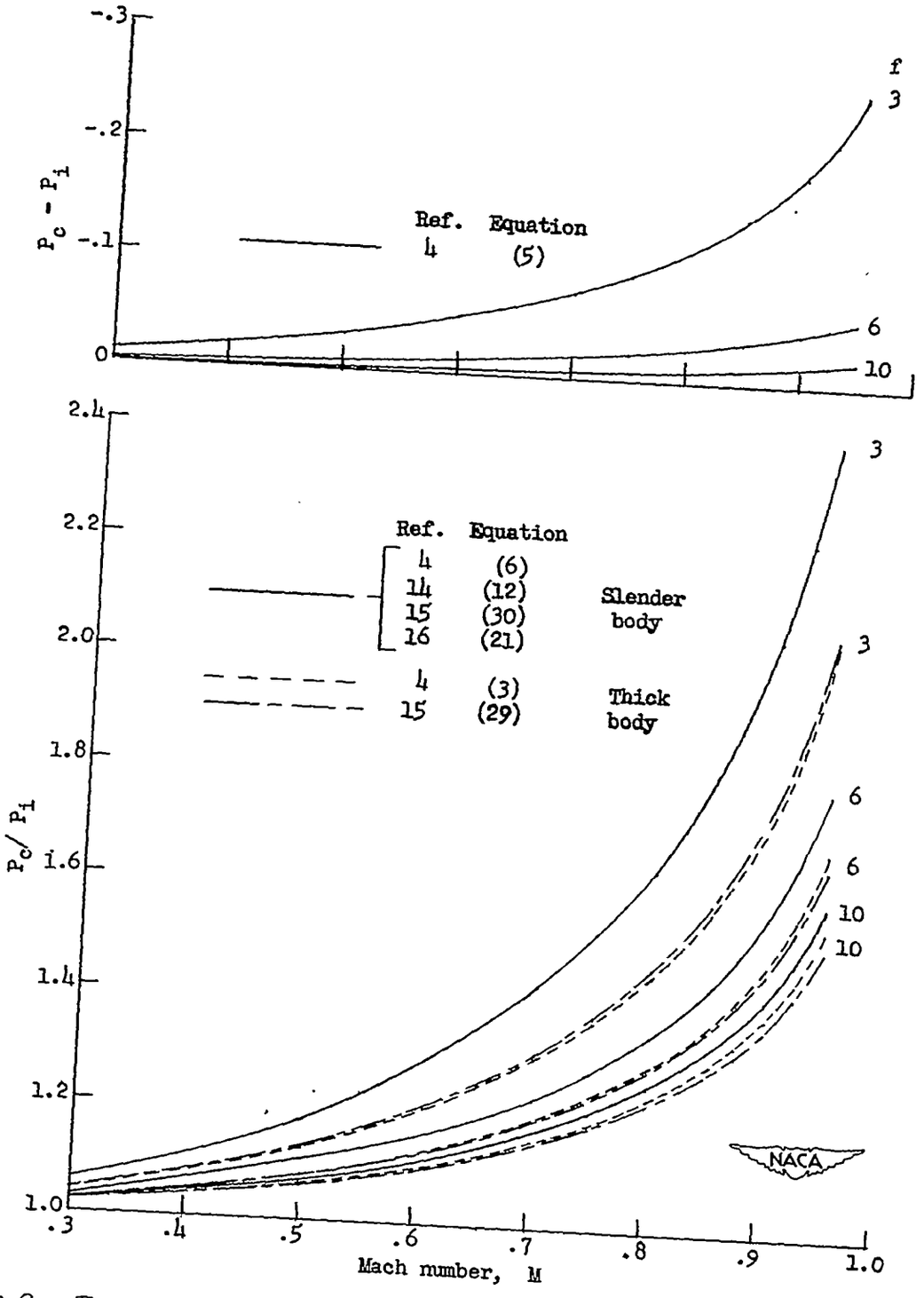

Figure 9.- Theoretical Mach number corrections for several prolate spheroids.

Security Classification of This Report Has Been Cancelled

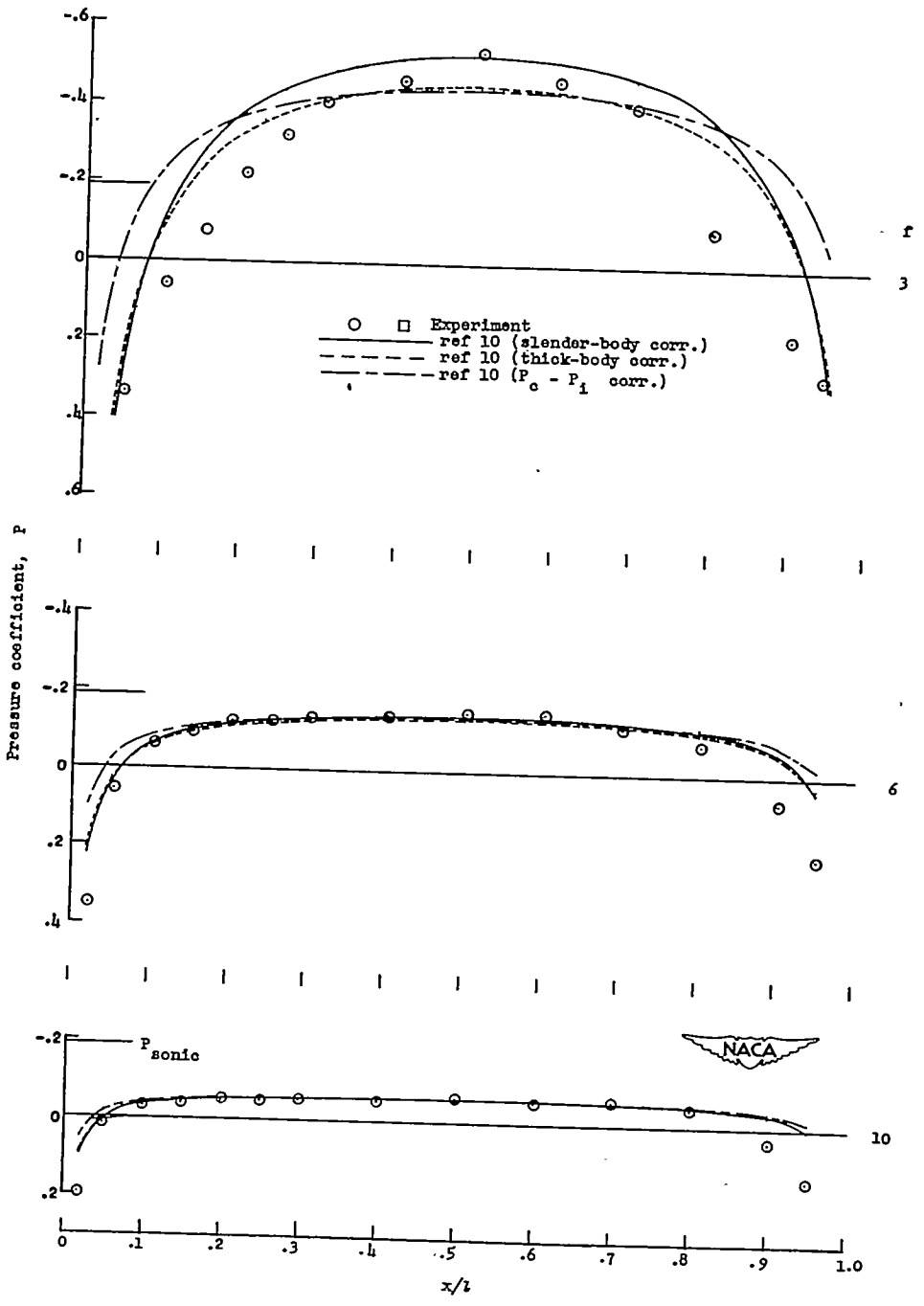

(a) $\alpha = 0^{\circ}$.

Figure 10.- Comparison of theoretical and experimental pressure distributions over the 0° and 180° meridians of several prolate spheroids. M = 0.90.

Security Classification of This Report Has Been Cancelled

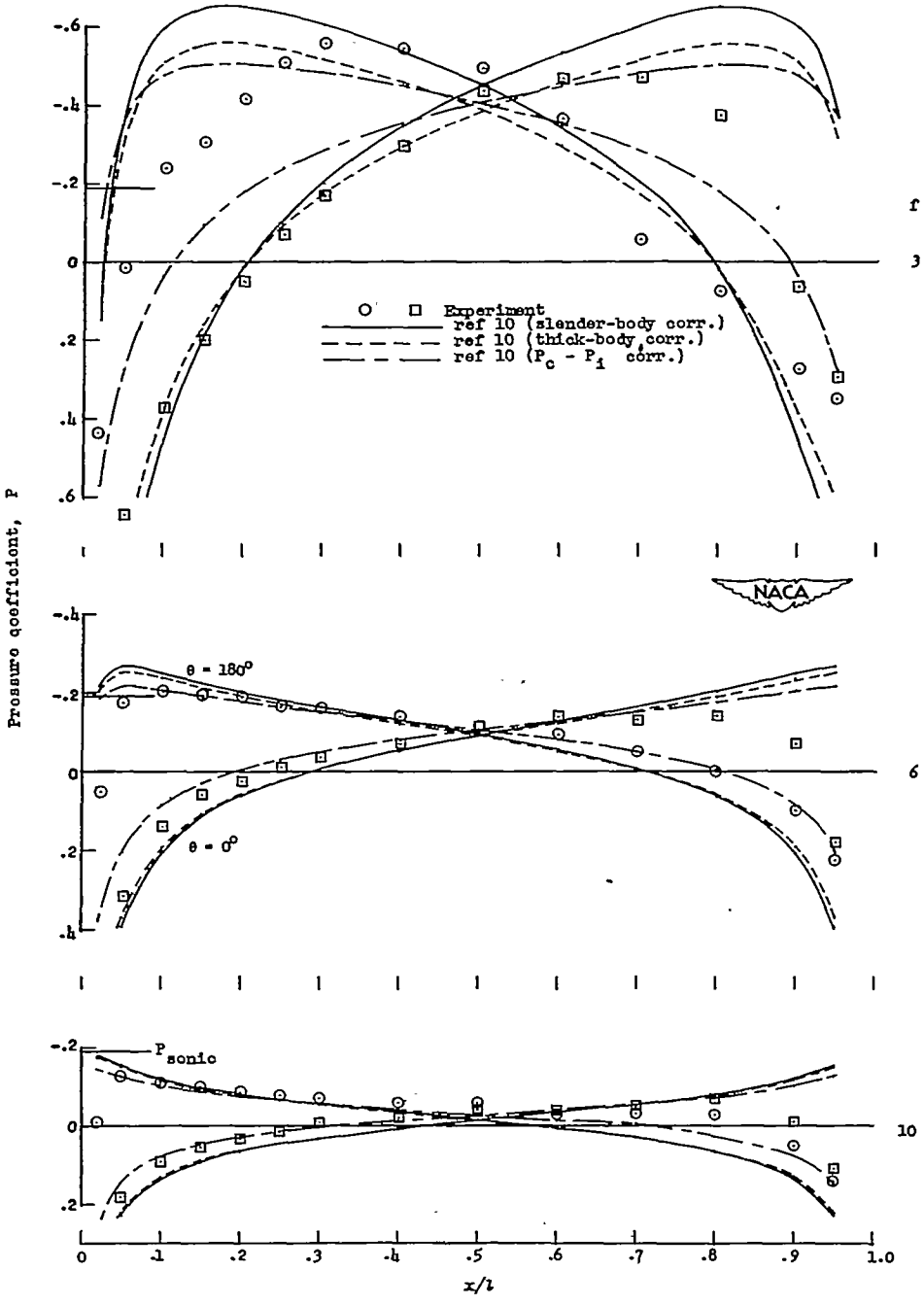

(b) $\alpha = 10^{\circ}$.

Figure 10.- Continued.

Security Classification of This Report Has Been Cancelled

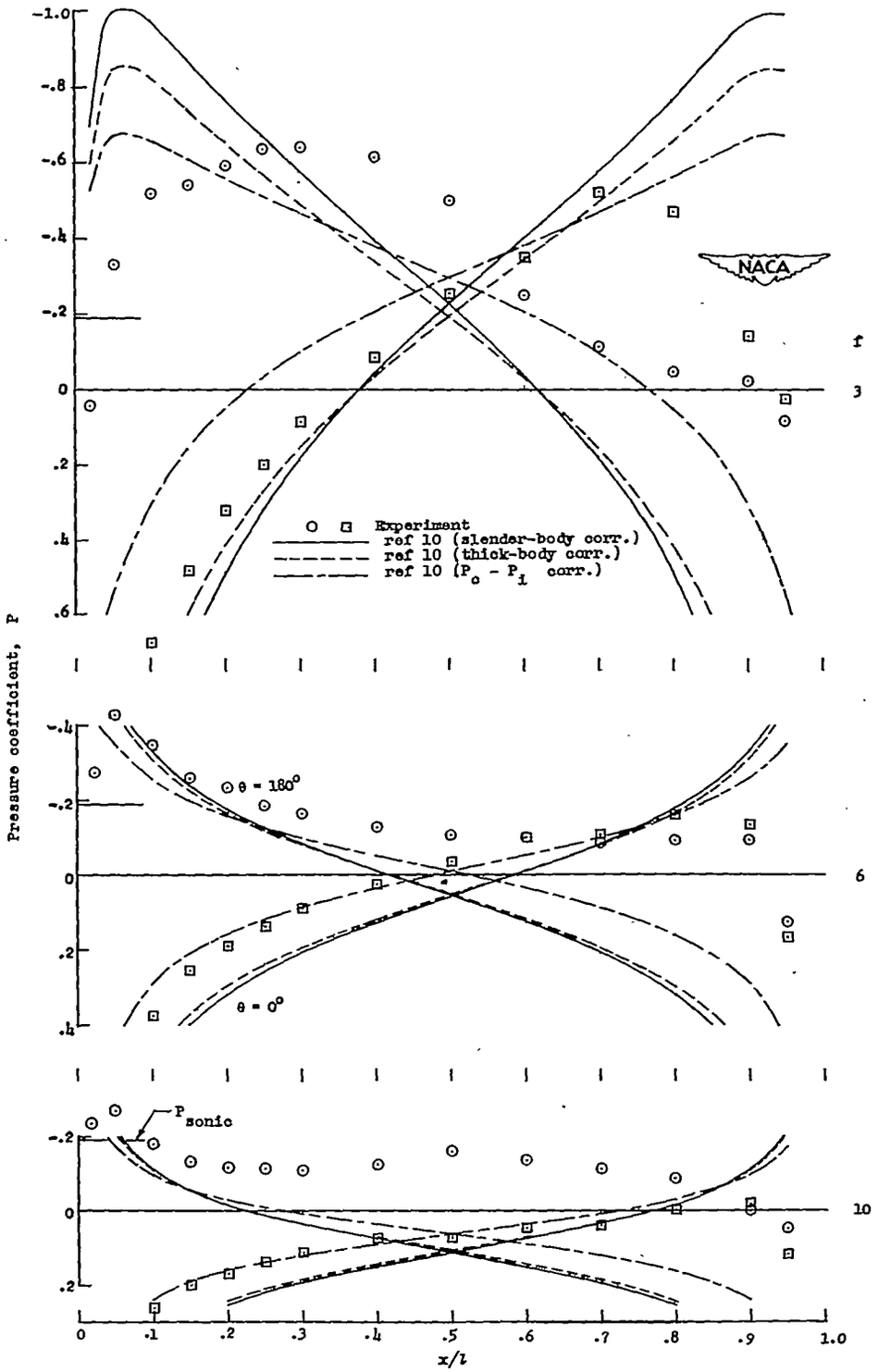

(c) $\alpha = 20^{\circ}$.

Figure 10.- Continued.

Security Classification of This Report Has Been Cancelled

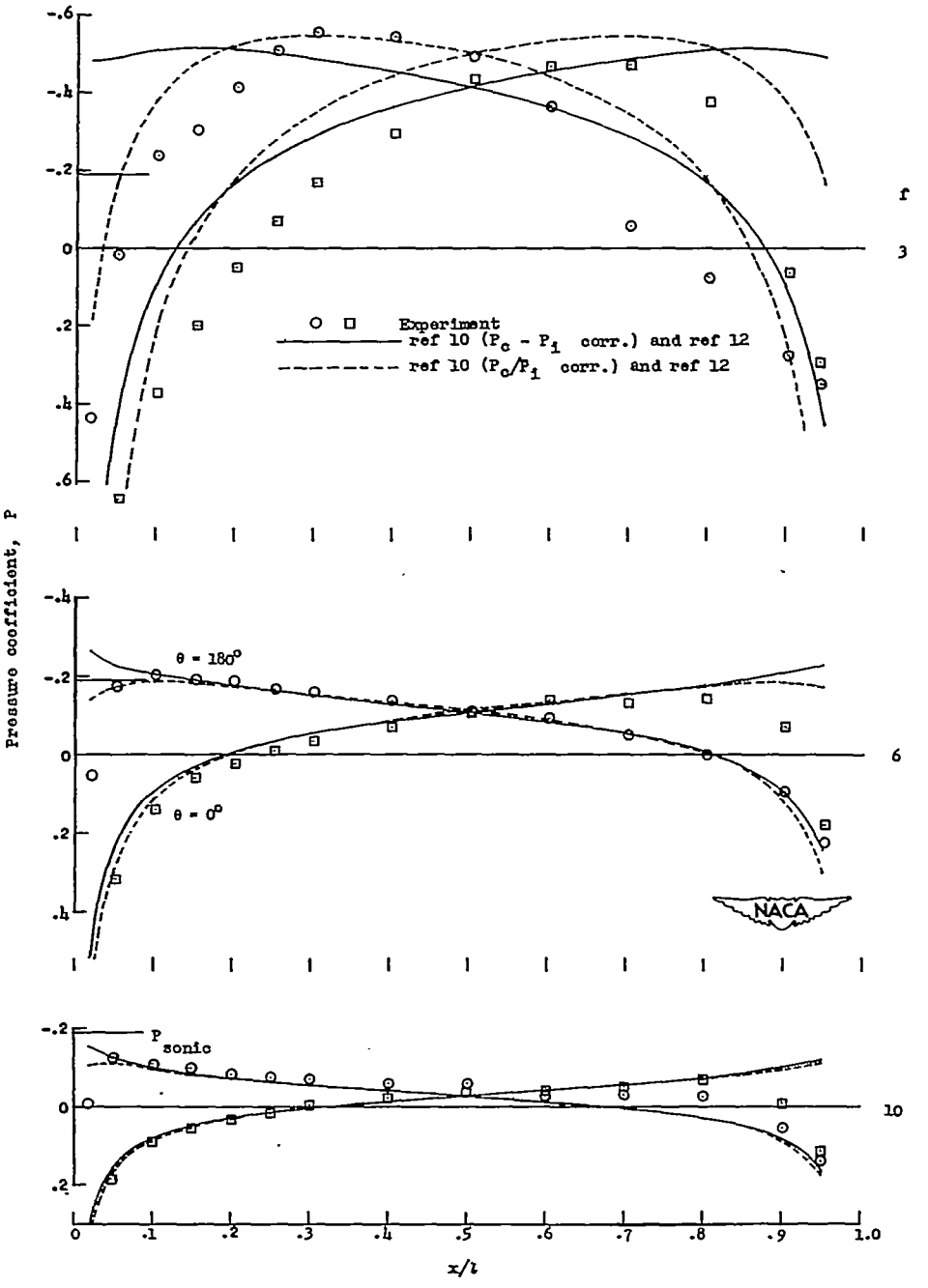

(d) $\alpha = 10^{\circ}$.

Figure 10.- Continued.

Security Classification of This Report Has Been Cancelled

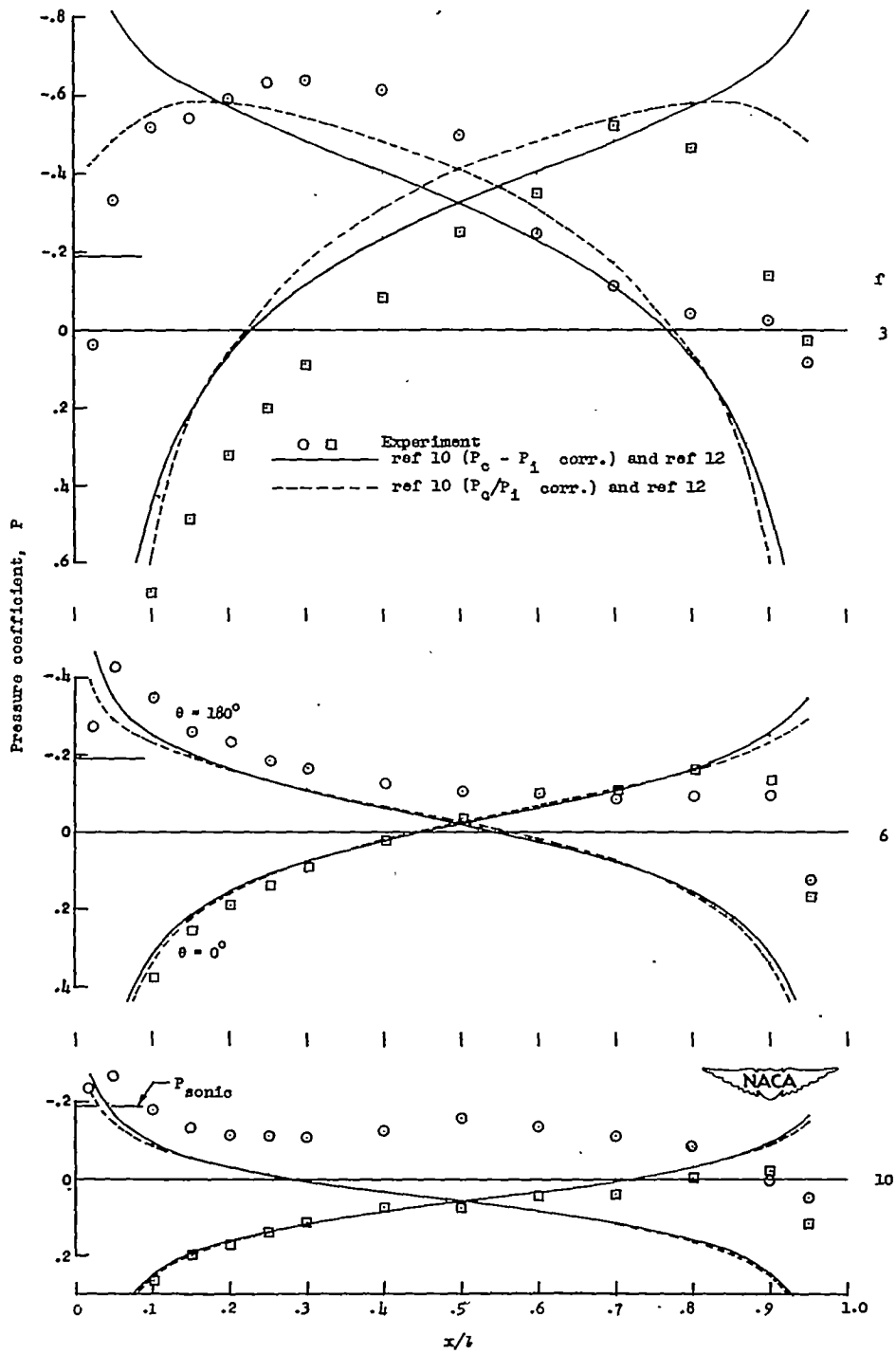

(e) $\alpha = 20^{\circ}$.

Figure 10.- Continued.

Security Classification of This Report Has Been Cancelled

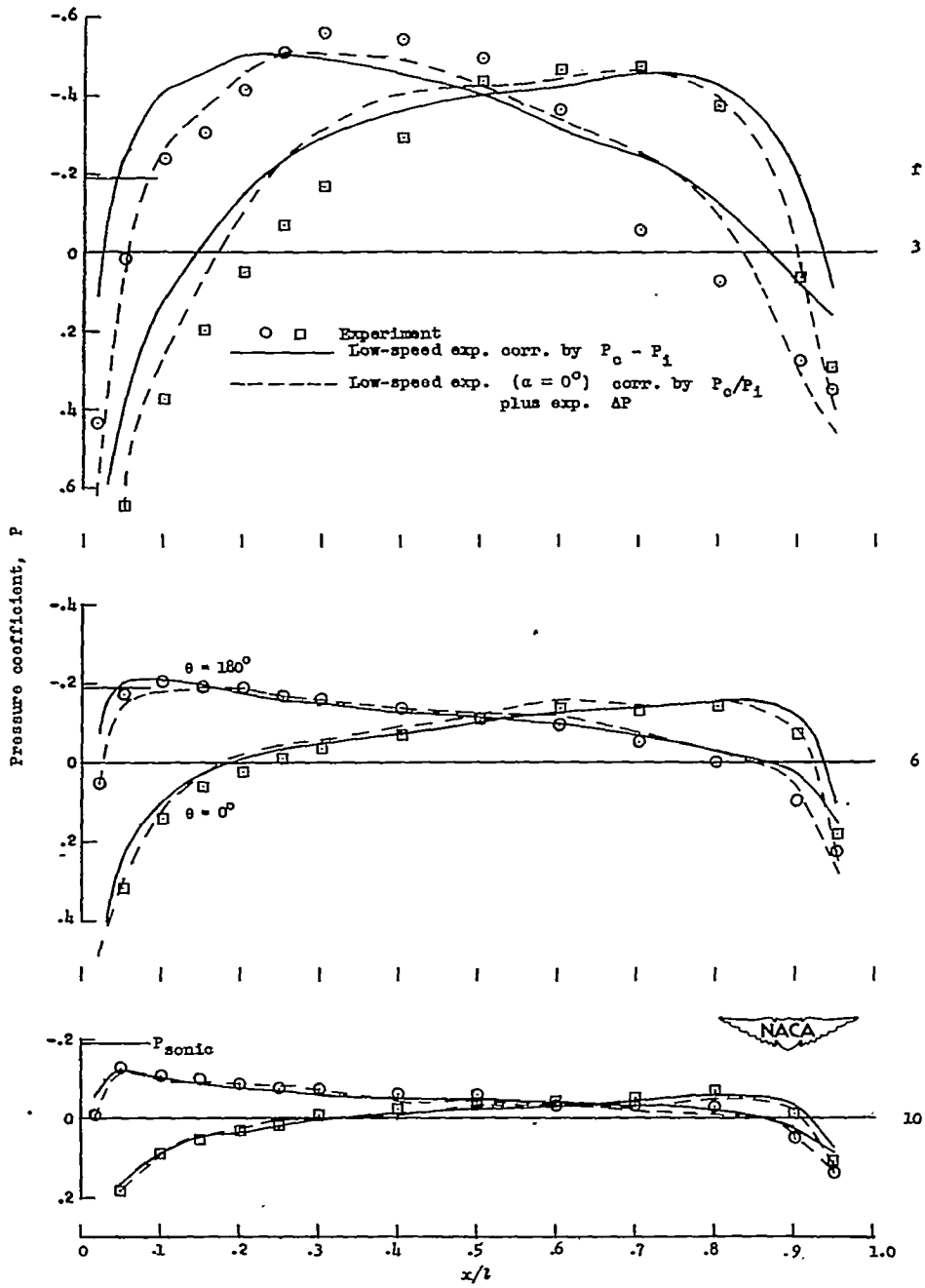

(f) $\alpha = 10^\circ$.

Figure 10.- Continued.

Security Classification of This Report Has Been Cancelled

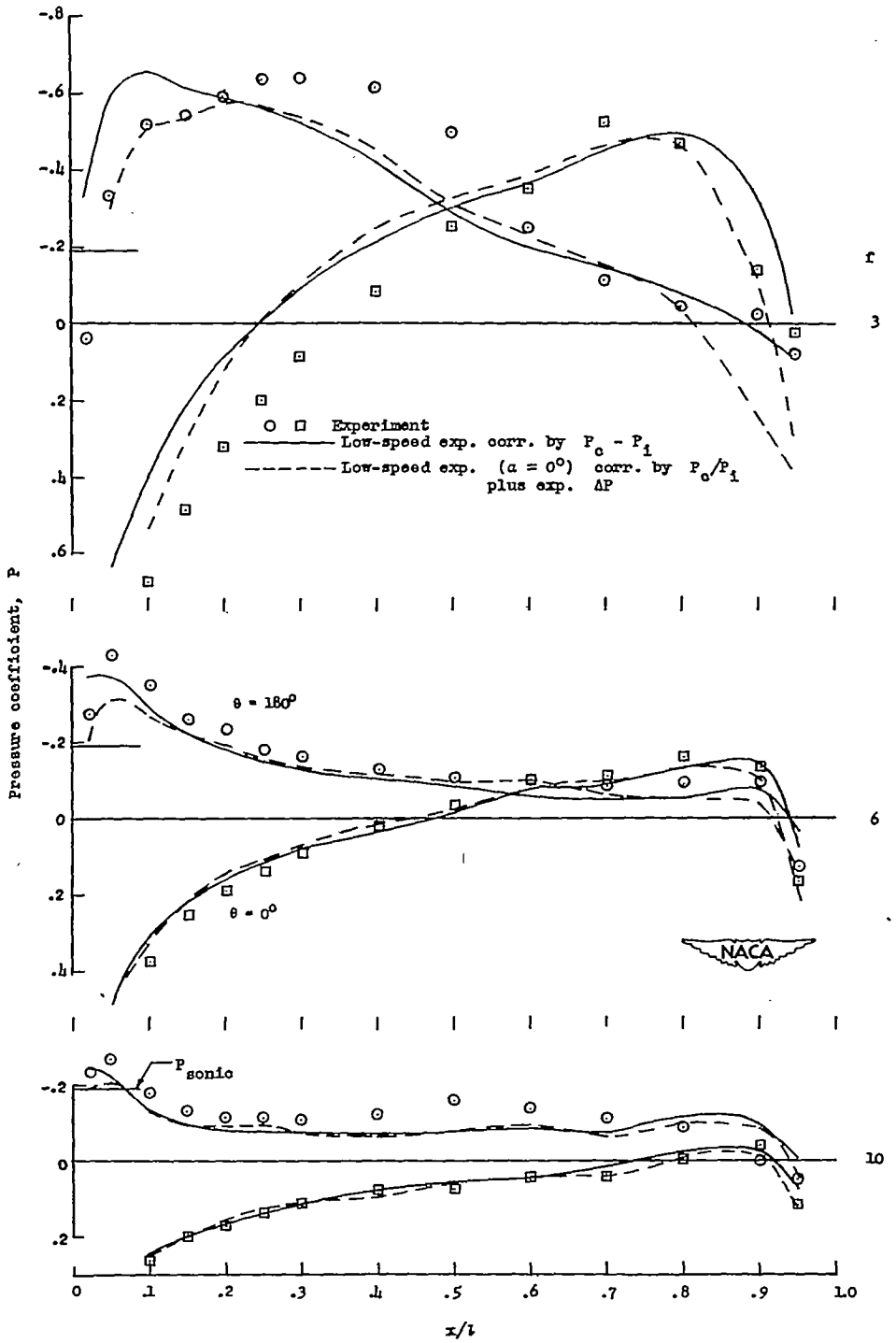

(g) $\alpha = 20^\circ$.

Figure 10.- Concluded.

Security Classification of This Report Has Been Cancelled

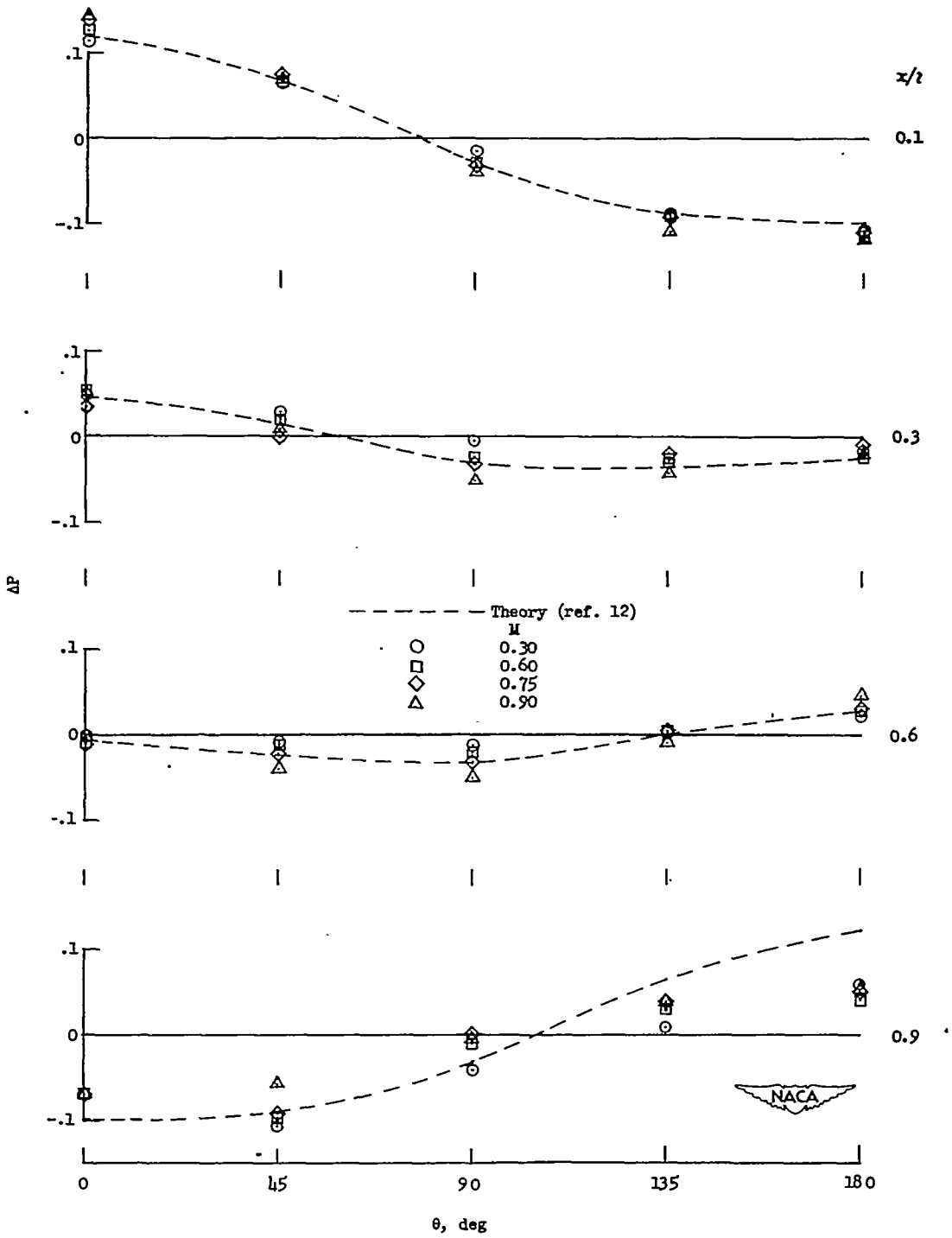

(a) f = 5.

Figure 11.- Theoretical and experimental incremental pressure coefficient around two prolate spheroids at $\alpha = 6^{\circ}$.

Security Classification of This Report Has Been Cancelled

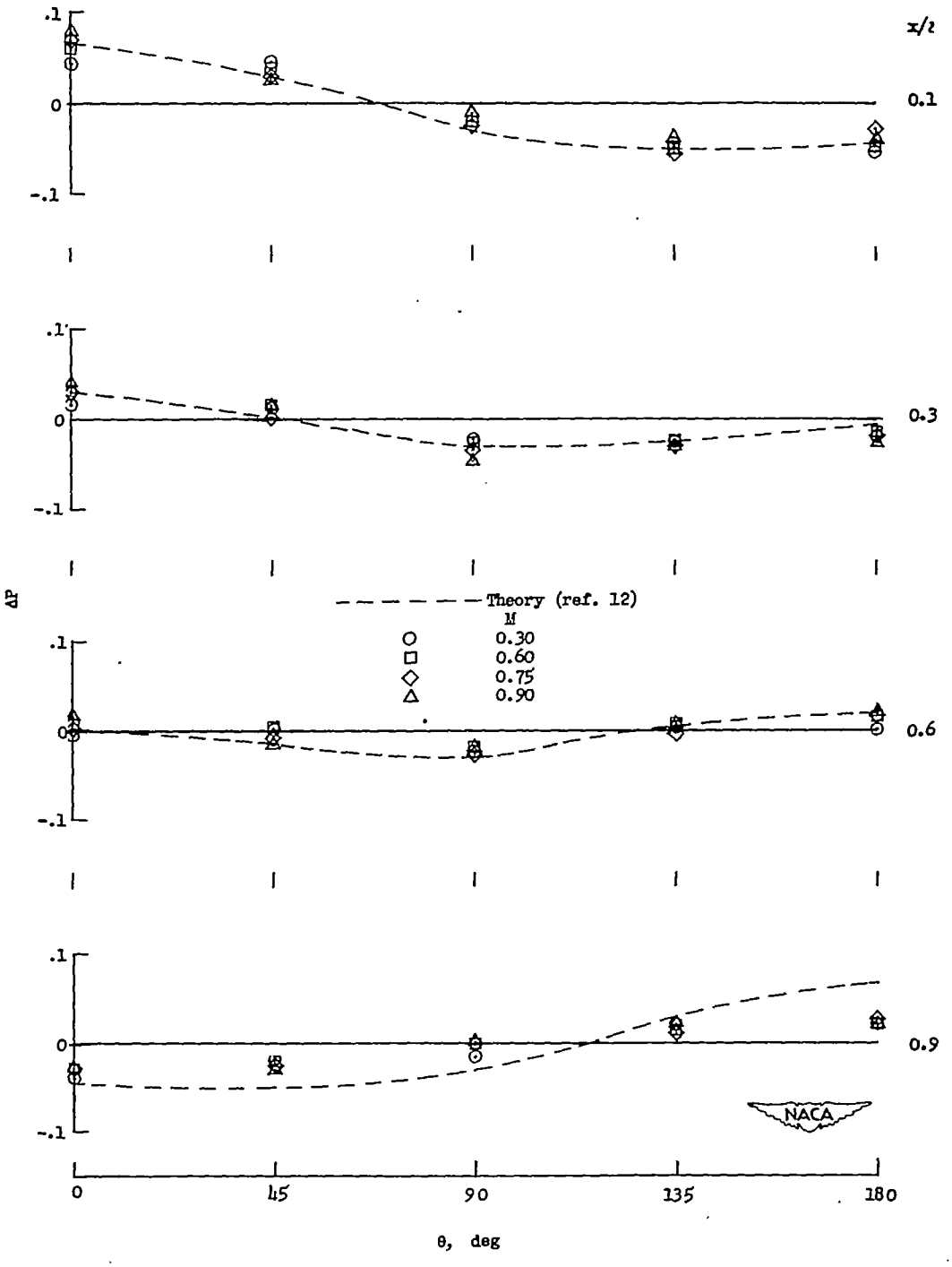

(b) f = 10.

Figure 11.- Concluded.

Security Classification of This Report Has Been Cancelled

CONFIDENTIAL

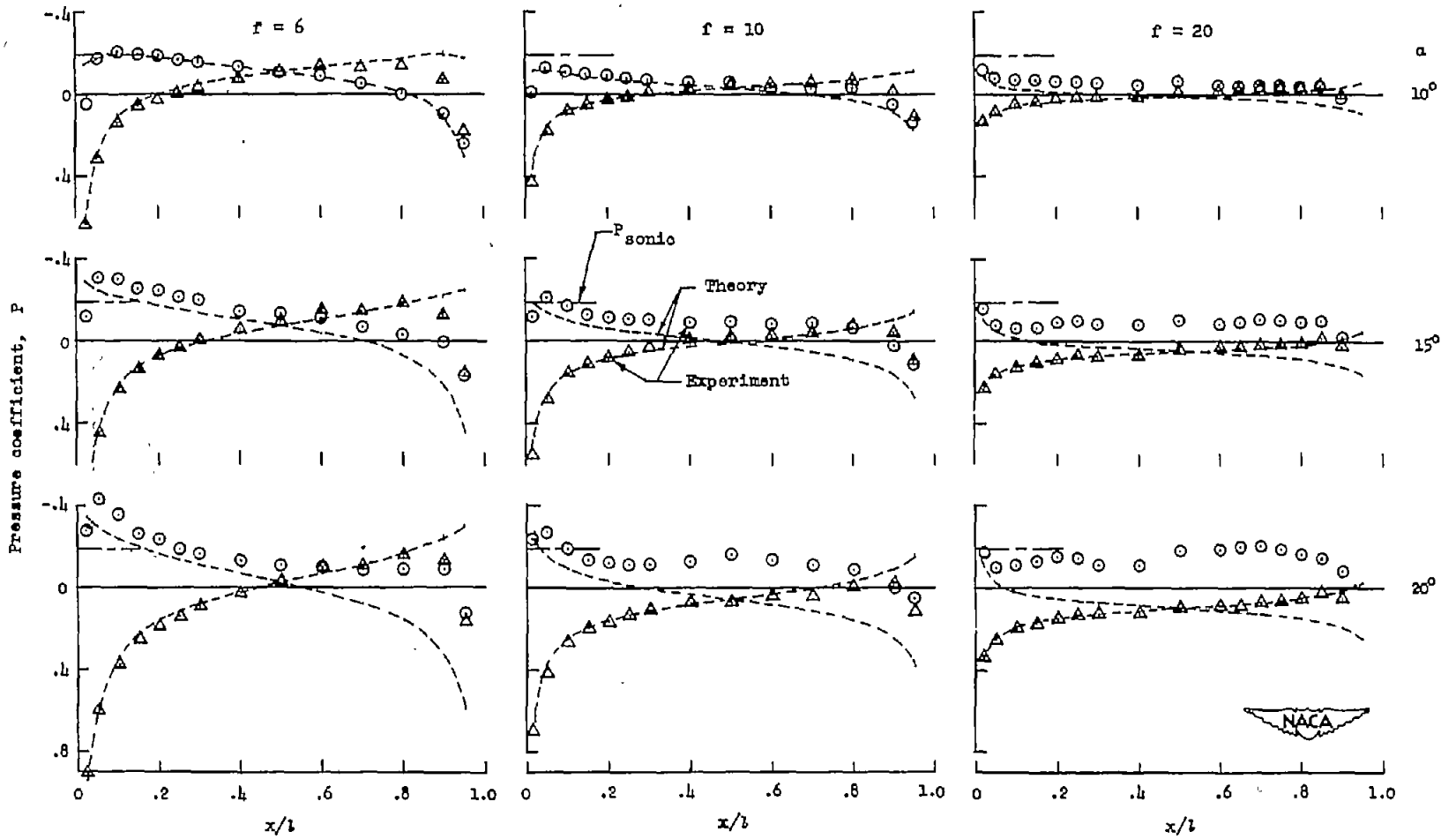

Figure 12.- Effect of fineness ratio and angle of attack on the approximate location of separation on the prolate spheroids. M = 0.9.

CONFIDENTIAL

Security Classification of This Report Has Been Cancelled

CONFIDENTIAL

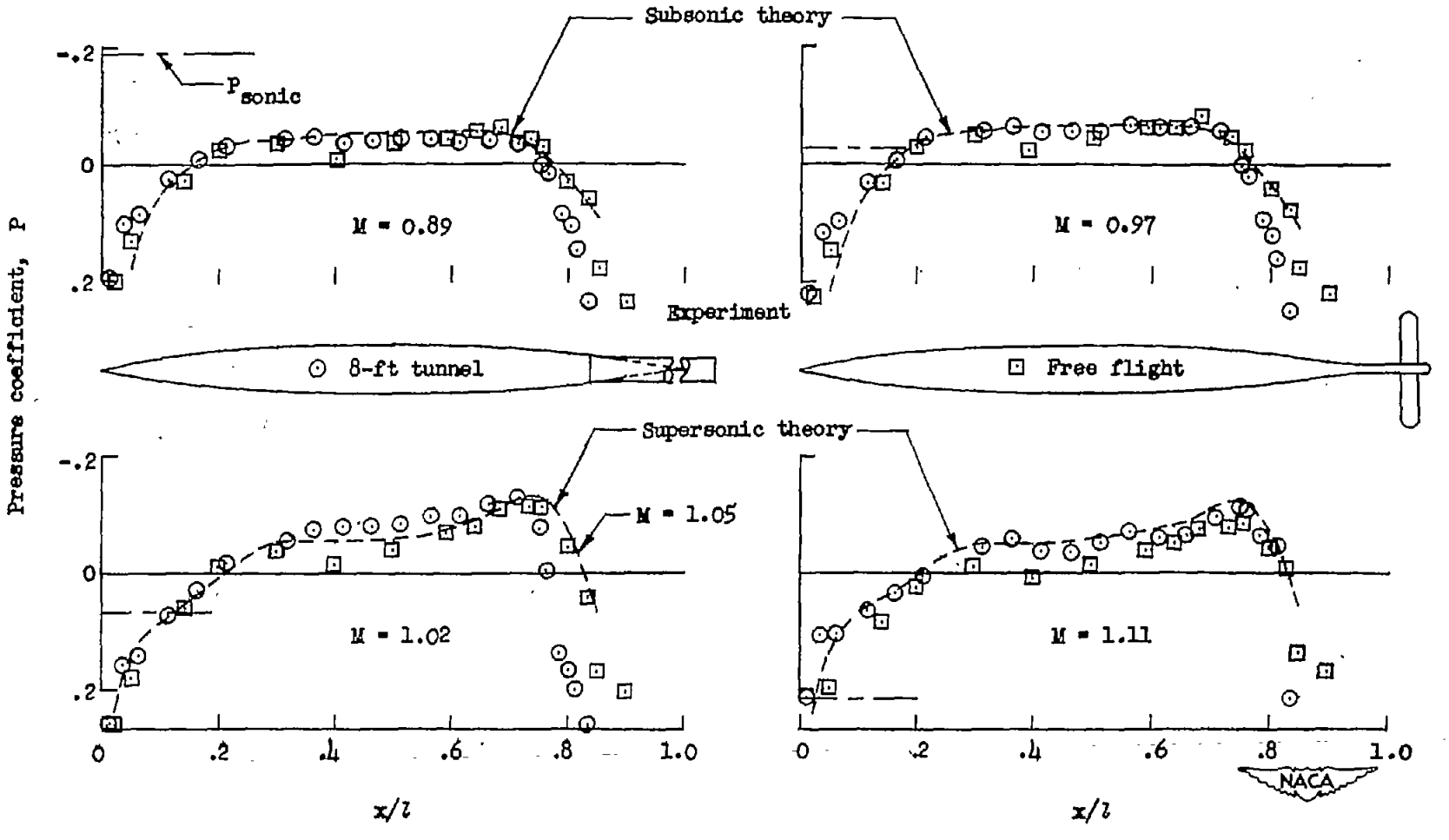

Figure 13.- Comparison of theoretical and experimental pressure distributions along the modified parabolic body at transonic speeds. $\alpha = 0^{\circ}$.

CONFIDENTIAL

Security Classification of This Report Has Been Cancelled

CONFIDENTIAL

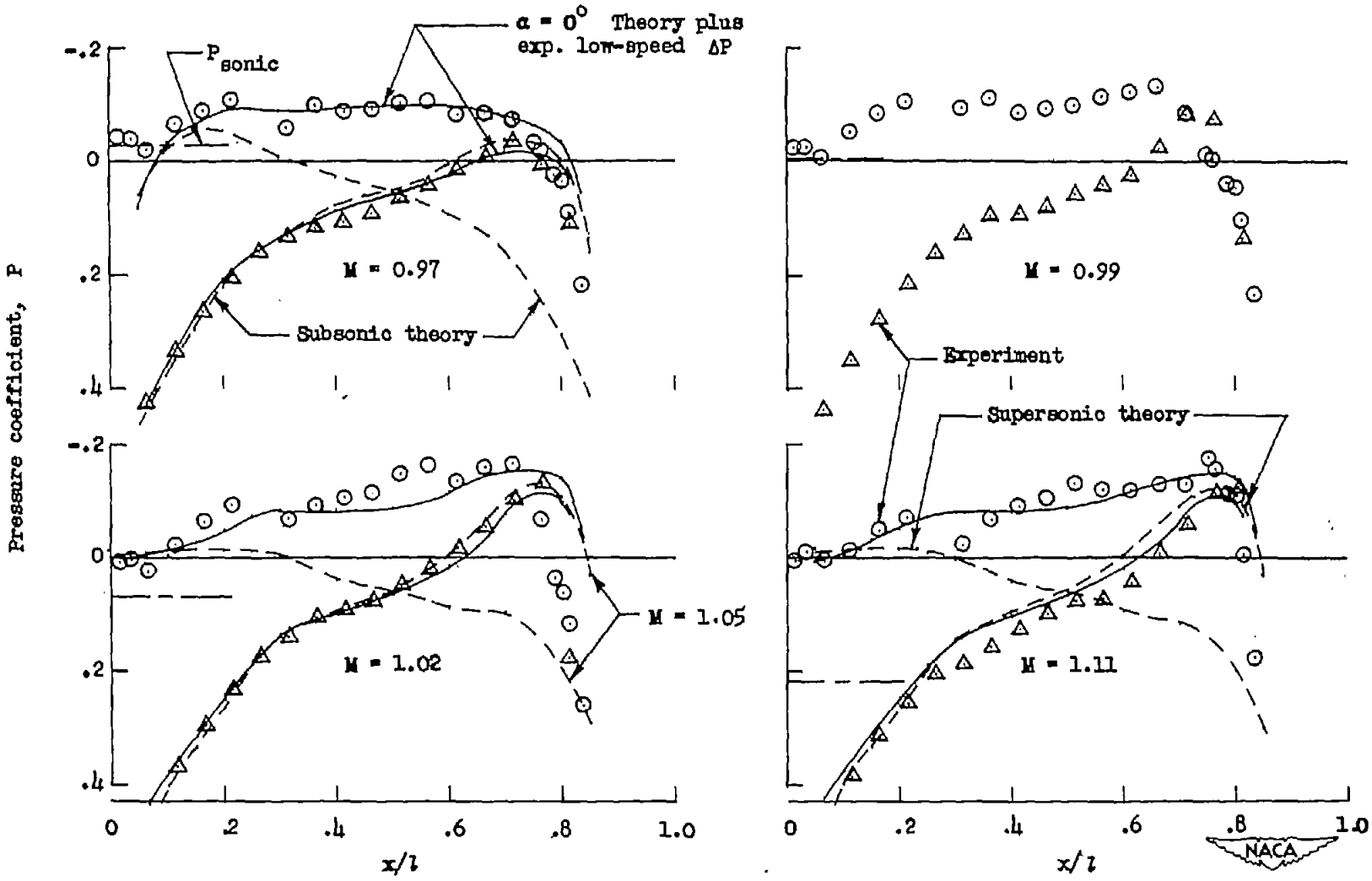

Figure 14.- Comparison of theoretical and experimental pressure distributions along the modified parabolic body at transonic speeds. $\alpha = 20^{\circ}$.

CONFIDENTIAL

Security Classification of This Report Has Been Cancelled

CONFIDENTIAL

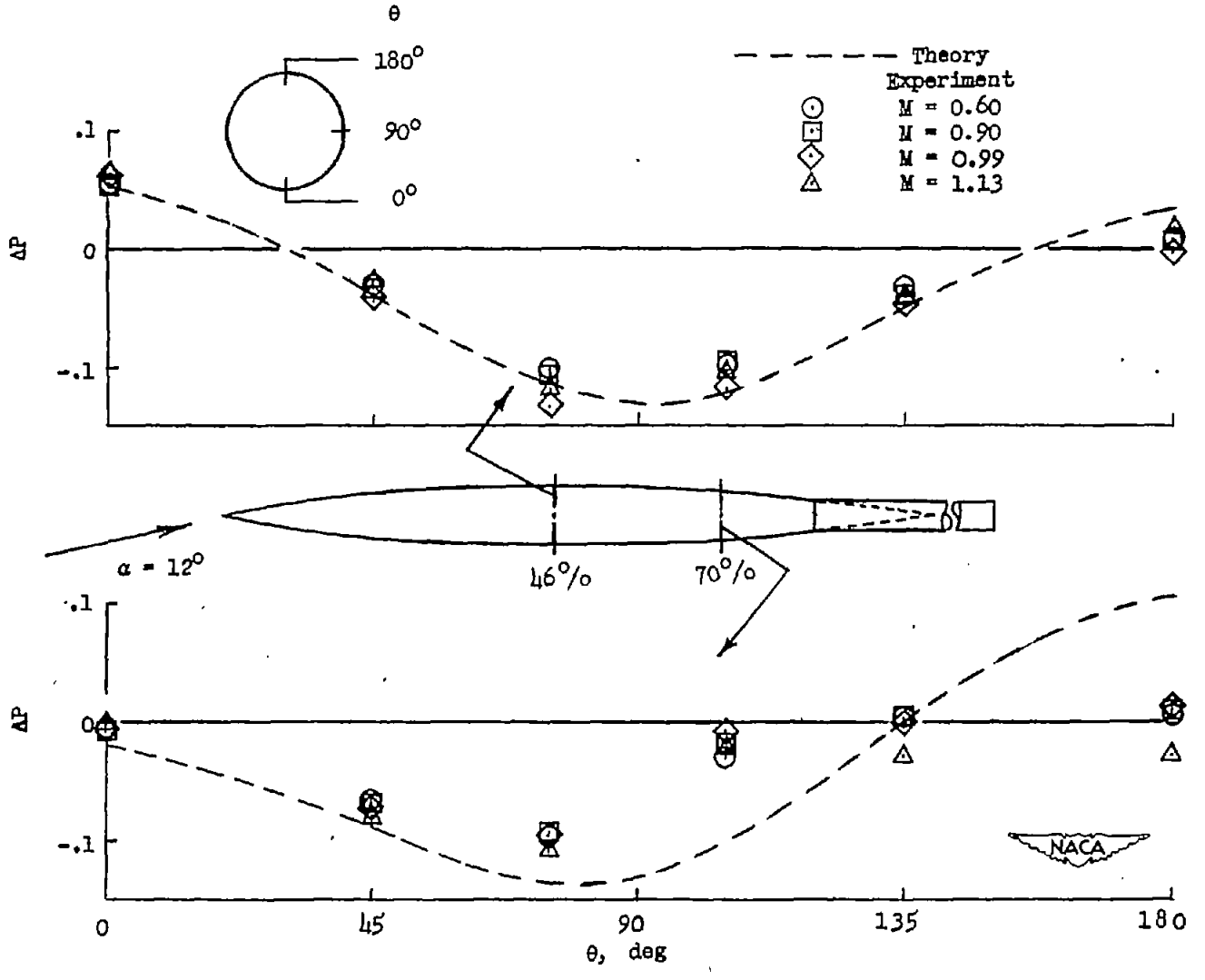

Figure 15.- Theoretical and experimental incremental pressure distributions around the modified parabolic body. $\alpha = 12^{\circ}$.

CONFIDENTIAL

NACA-Langley - 7-31-52 - 350